energies

MDPI

Article

Operational Analysis of a Pilot-Scale Plant for Hydrogen Production via an Electrolyser Powered by a Photovoltaic System

Lucio Bonaccorsi [1], Rosario Carbone [2], Fabio La Foresta [1,*], Concettina Marino [1], Antonino Nucara [1], Matilde Pietrafesa [1] and Mario Versaci [1]

[1] Department of Civil, Energetic, Environmental and Material Engineering, Mediterranea University of Reggio Calabria, Via Zehender, 89100 Reggio Calabria, Italy; lucio.bonaccorsi@unirc.it (L.B.); concettina.marino@unirc.it (C.M.); antonino.nucara@unirc.it (A.N.); matilde.pietrafesa@unirc.it (M.P.); mario.versaci@unirc.it (M.V.)

[2] Department of Information Engineering, Infrastructures and Sustainable Energy, Mediterranea University of Reggio Calabria, Via Zehender, 89100 Reggio Calabria, Italy; rosario.carbone@unirc.it

* Correspondence: fabio.laforesta@unirc.it

Abstract

This study presents preliminary findings from an experimental campaign conducted on a pilot-scale green hydrogen production plant powered by a photovoltaic (PV) system. The integrated setup, implemented at the University "Mediterranea" of Reggio Calabria, includes renewable energy generation, hydrogen production via electrolysis, on-site storage, and reconversion through fuel cells. The investigation assessed system performance under different configurations (on-grid and selective stand-alone modes), focusing on key operational phases such as inerting, purging, pressurization, hydrogen generation, and depressurization. Results indicate a strong linear correlation between the electrolyser's power setpoint and the pressure rise rate, with a maximum gradient of 0.236 bar/min observed at 75% power input. The system demonstrated robust and stable operation, efficient control of shutdown sequences, and effective integration with PV input. These outcomes support the technical feasibility of small-scale hydrogen systems driven by renewables and offer valuable reference data for calibration models and future optimization strategies.

Keywords: green hydrogen; electrolysis; photovoltaic system; energy storage; fuel cell

Academic Editors: Kai Song, Jin Lin, Fulin Fan and Jinhai Jiang

Received: 25 June 2025
Revised: 21 July 2025
Accepted: 21 July 2025
Published: 24 July 2025

Citation: Bonaccorsi, L.; Carbone, R.; La Foresta, F.; Marino, C.; Nucara, A.; Pietrafesa, M.; Versaci, M. Operational Analysis of a Pilot-Scale Plant for Hydrogen Production via an Electrolyser Powered by a Photovoltaic System. *Energies* **2025**, *18*, 3949. https://doi.org/10.3390/en18153949

1. Introduction

The transition toward a sustainable energy future requires the development of efficient technologies for the production and storage of clean energy carriers, with hydrogen playing a pivotal role. Traditional methods for hydrogen generation, however, are typically energy-intensive and rely on fossil fuels such as natural gas, coal, and oil. These processes are associated with significant greenhouse gas emissions and contribute substantially to the global carbon footprint. In contrast, the integration of renewable energy sources in the hydrogen production pathway may offer a cleaner alternative. Specifically, green hydrogen, produced through water electrolysis powered by renewables like photovoltaic or wind systems, represents a promising integrated solution [1,2].

Despite its potential, the economic competitiveness of green hydrogen and its impact on traditional energy markets still require further investigation. The successful integration of this technology also depends on regulatory advancements and the evolution of supporting infrastructure. Nevertheless, green hydrogen could mitigate the intermittency of

renewable sources and foster new energy market opportunities [3]. Therefore, the application and advancement of water electrolysis technology is regarded as a viable strategy for achieving partial or full decarbonization of the energy sector [4].

Water electrolysis has long been employed for hydrogen production and is currently available in three main technologies: solid oxide electrolyser (SOE), polymer electrolyte membrane (PEM), and alkaline water electrolyser (AWE) [3,5,6]. Among them, the AWE remains the most commercially adopted due to its maturity, longer lifespan, and relatively lower costs [5].

Many studies have examined renewable-powered electrolysis systems, often focusing on their energy performance [7–9] or addressing techno-economic aspects [10–13]. Research has also explored the use of green hydrogen for storage [14–17] and its reconversion into electricity through fuel cells [18,19] has been extensively investigated. Nevertheless, the majority of these works are theoretical and based on modelling approaches that simulate various components such as PV arrays, electrolysers, storage systems, and inverters [20–27].

In contrast, only a limited number of studies provide experimental analyses of integrated systems operating under real-world, variable conditions [28,29]. This study aims to fill that gap by presenting the experimental results from a pilot-scale hydrogen production plant powered by photovoltaics. The system includes energy storage, gas purification, and reconversion, and allows for multiple operational configurations. The novelty of this work lies in its real-world implementation, the dynamic control logic managing critical process phases, and the high-resolution monitoring of both process and environmental parameters.

Compared to previous experimental works, which demonstrated the feasibility of continuous hydrogen production under varying solar conditions, using a very small-scale PV-electrolysis test system [9,30,31], the proposed analysis focuses on a fully developed prototype whose size and complexity are not common in previous studies, providing insight into the real-time control of an integrated hydrogen system. Furthermore, unlike techno-economic studies regarding hydrogen integration into grid-connected or renewable energy communities [32,33], this work offers a fully experimental perspective, providing empirical data to support simulation-based planning and optimization efforts.

Within this framework, the present study aims to analyze and experimentally evaluate a pilot-scale integrated plant for hydrogen production, storage, and reconversion, located at the Energy and Environment Laboratory of the DICEAM Department, University "Mediterranea" of Reggio Calabria. The study focuses on technical behaviour under different operational configurations, control logic, and the identification of performance indicators useful for modelling and optimization. The plant is a complex, integrated system, organized into several functional sections: the renewable energy section (including a photovoltaic array, wind turbines, inverters, and storage batteries), the power conditioning section, the production section (based on an electrolyser), the purification section, the reconversion section (comprising fuel cells and associated batteries/inverters), the control section, and the monitoring section. The main components are housed in a dedicated container to ensure safe and efficient management.

The main objectives of the analysis conducted in this work were the following:

- to experimentally evaluate the main parameters of the process and energy flows under real climatic conditions, with particular attention to solar radiation;
- to identify inefficiencies affecting the plant's overall energy performance, with a focus on critical components such as the electrolyser, storage systems, and fuel cell;
- to provide valuable data for future optimization efforts and for the calibration of simulation models.

To pursue these goals, an experimental measurement campaign was carried out under different operating configurations, aimed at analyzing system performance and acquiring

data on both process and environmental parameters. Continuous monitoring included variables such as hydrogen pressure, ambient temperature, as well as voltage, current, and power delivered to the electrolyser, along with data from the photovoltaic generator and meteorological conditions.

The analysis of the collected data enabled a detailed characterization of the system's behaviour across its various operational phases (startup, inerting, standby, pre-start, purging, pressurization, production, shutdown, depressurization), and revealed key correlations between the rate of pressure increase during the pressurization phase and the power setpoint applied to the electrolyser.

The findings from this study are essential for the subsequent development of the research, which aims to optimize the prototype system in response to varying climatic conditions and load scenarios. Furthermore, the outcomes will support the development of operational procedures and simulation models to assess the scalability of the prototype for deployment in different operational contexts. This paper provides a comprehensive description of the plant, the experimental methodology, and the main results, laying the groundwork for assessing the performance and guiding the future optimization of the integrated hydrogen-renewable energy system.

2. Overview of the Integrated Hydrogen Production System

The system under analysis is divided into several main sections, each comprising specific components dedicated to a particular function within the hydrogen production, storage, and reconversion process. The core equipment is housed within a container to ensure simplified and safe management (Figure 1).

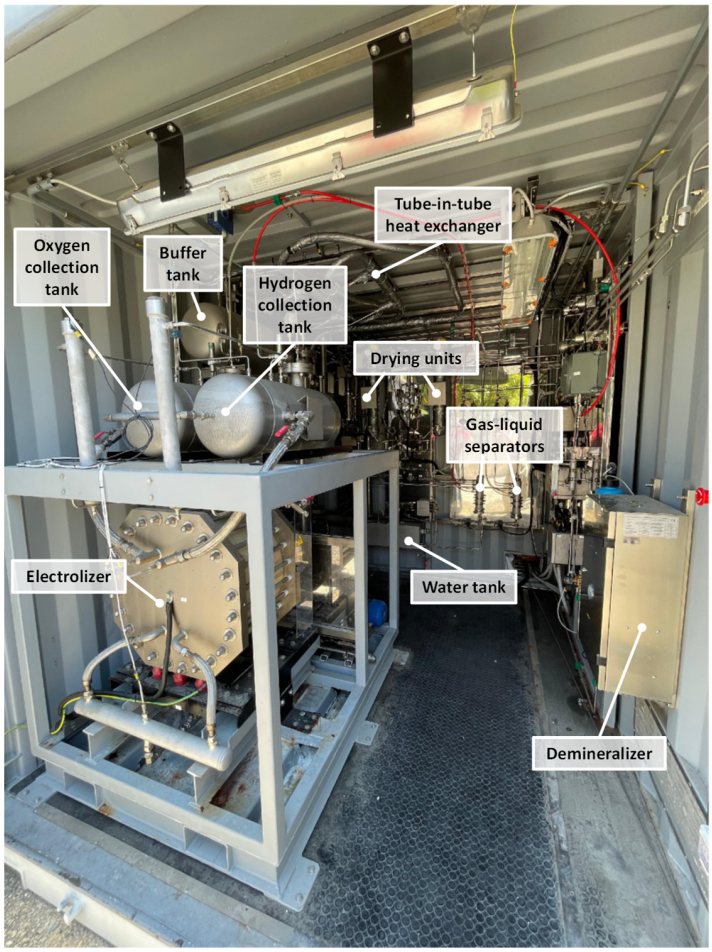

Figure 1. Arrangement of the main component of the plant.

The main sections that make up the plant are as follows:

- Photovoltaic energy section
- Power conditioning section
- Hydrogen production and purification sections
- Reconversion section
- Control section
- Monitoring section

All sections interact synergistically to create a complete system for hydrogen production, storage, and utilization, designed to operate efficiently, safely, and sustainably.

In the following subsections, each part of the system is described in detail.

2.1. Photovoltaic Energy Section

This part of the system is dedicated to generating energy from renewable sources, primarily to power the electrolyser. It includes the components reported in the following list (see also Figure 2).

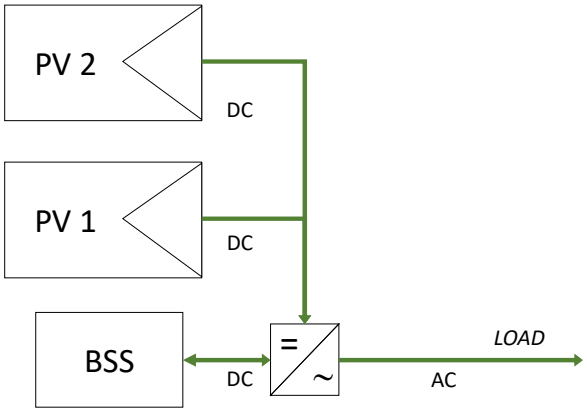

Figure 2. Photovoltaic energy section scheme.

- Photovoltaic Array (PV). It consists of two strings (PV1 and PV2) of monocrystalline silicon solar panels connected in parallel. Each string includes 9 modules in series, with a total peak power output of 6.48 kWp.
- Hybrid Inverter (HI). It is a multifunctional device that manages the produced electrical energy, functioning both as an MPPT (Maximum Power Point Tracker) regulator and as an inverter to supply the electrolyser and/or to charge the batteries. It has a rated power of 6 kW.
- Battery Storage System (BSS). The bank is made of five 48 V, 50 Ah lithium batteries connected in series to provide a total of 240 V and 12 kWh of energy storage.

2.2. Power Conditioning Section

The power conditioning section regulates the DC power supply to the electrolyser, ensuring it is properly adjusted to meet the operational requirements of the device. As a matter of fact, the direct current (DC) produced by the photovoltaic field is converted into alternating current (AC) by the hybrid inverter of the photovoltaic energy section, to make it available for the loads. However, the portion of power supplied to the electrolyser must be converted back into direct current (DC).

Therefore, this conditioning section handles the conversion of electrical energy from alternating current (AC) to direct current (DC), which is required for the operation of the electrolyser. The power supply consists of the following:

- a power electronic converter, composed of a transformer and a diode rectifier, which supplies direct current with a maximum voltage of 72 V at a rated current of 200 A;
- a power electronic control system, responsible for stabilizing the converter's output current, also according to the user's setting.

2.3. Hydrogen Production Section

This is the core of the system, where the actual production of hydrogen and oxygen takes place through electrolysis. The following equipment is included in this section (Figure 3):

- Electrolyser (EM), which splits water into hydrogen and oxygen using a potassium hydroxide (KOH) solution as the electrolyte. It can produce up to 2 Nm^3/h of H_2 and 1 Nm^3/h of O_2, operating between 2 and 10 kW and reaching pressures up to 20 bar.
- Hydrogen and oxygen collection tanks (HV and OV), where the generated gases are temporarily stored before being vented or sent to purification.
- Heat exchangers (HE and OE), tube-in-tube type, that reduce the temperature of the produced gases.
- Bubblers (HW and OW), which remove impurities such as moisture and residual gases from the produced hydrogen and oxygen.
- Gas–liquid separators (HS and OS), which recover residual water from the gas streams and send it back to the makeup water tank.
- Demineralizer (WU), where tap water is treated to make it suitable for electrolysis.
- Makeup water tank (WT), with a capacity of 15 L of demineralized water, which ensures continuous water supply to the electrolyser.
- Cooling system, consisting of a circulation pump, a 200 L buffer tank, and a 7.3 kW chiller, which removes the heat generated during electrolysis.

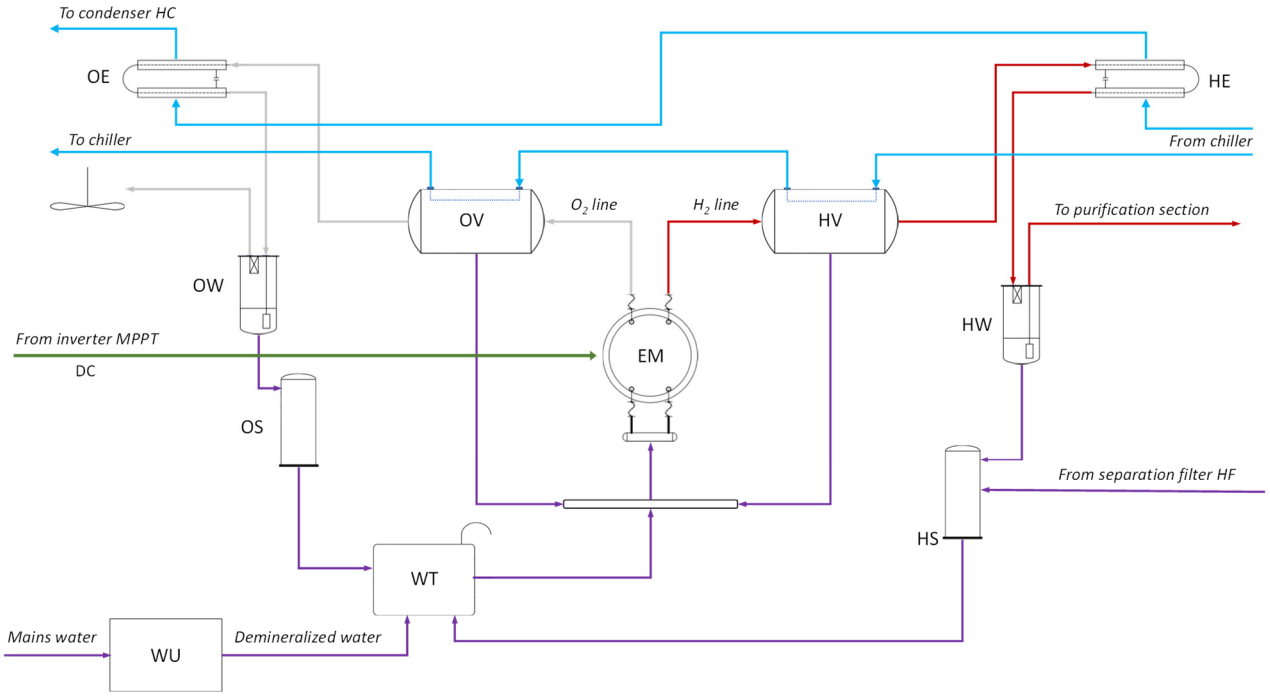

Figure 3. Hydrogen production section scheme.

2.4. Purification Section

In this section, the hydrogen produced is purified to reach a concentration of 99.99%, making it suitable for use in the fuel cell. The following equipment is included in this section (Figure 4):

- Buffer tank (HD), a stainless-steel vessel where hydrogen is temporarily stored before the purification process.
- Catalytic deoxidation reactor (HDO), which removes residual oxygen by inducing a reaction with excess hydrogen to form water vapour.
- Condenser (HC), which cools and condenses the vapour generated during the deoxidation reaction.
- Separation filter (HF), which removes the condensed water using a coalescing filter.
- Drying units (DR-A and DR-B), which operate alternately to remove residual moisture from the gas stream.
- Storage tank (HB), which is a 0.70 m^3 stainless steel tank used to collect the purified hydrogen.

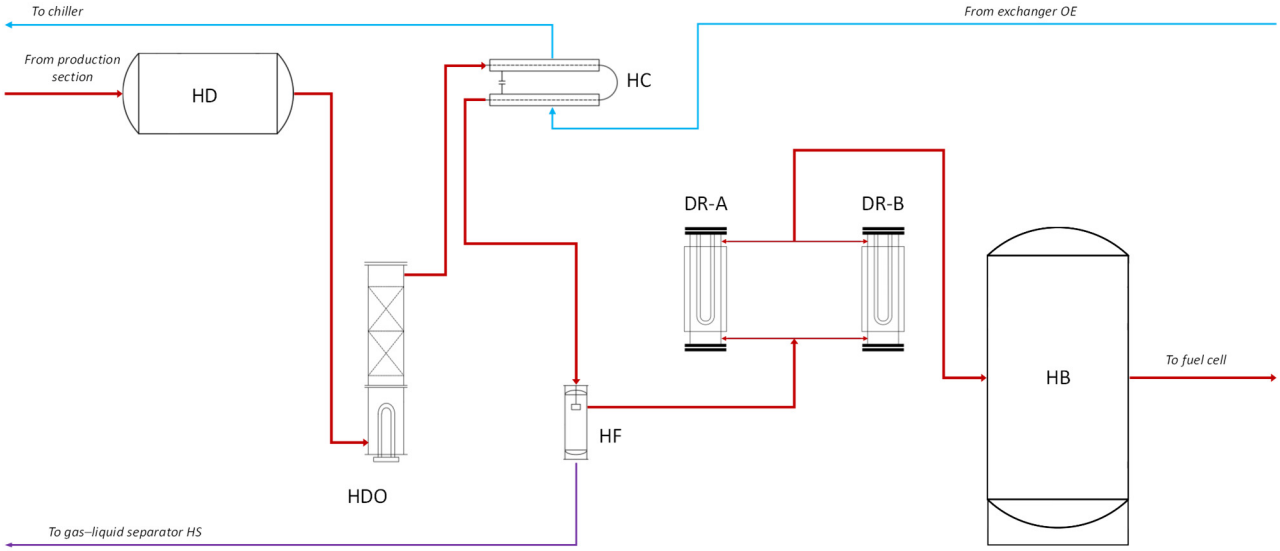

Figure 4. Purification section scheme.

2.5. Reconversion Section

In this section, the stored hydrogen is reconverted into electrical energy. The main components are the following (Figure 5):

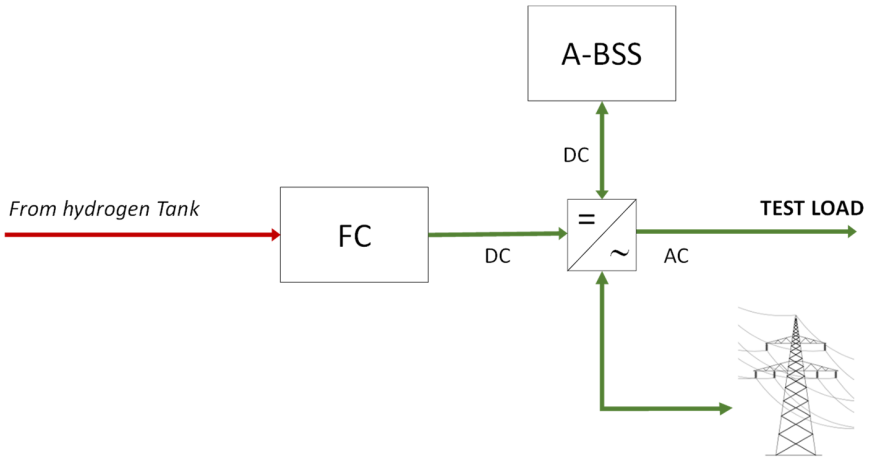

Figure 5. Reconversion section scheme.

- fuel cell (FC), PEM type, with a nominal power output of 1.7 kW in direct current (DC);
- multifunction inverter—it manages both the conversion from DC to AC for loads and the charging of the auxiliary battery pack (A-BSS);
- Auxiliary battery storage system (A-BSS), with a nominal voltage of 48 V and a rated capacity of 368 Ah.

2.6. Control Section

This section is dedicated to the monitoring and control of all system operating parameters. The control is managed through a Programmable Logic Controller (PLC) interface, housed in a dedicated control cabinet that includes the following:

- control buttons (Reset, Emergency Stop, Start);
- indicator lights for process supervision;
- alarm management and safety sequence control.

2.7. Monitoring Section

This section is devoted to the monitoring of parameters relevant to the analysis of the renewable energy production system's efficiency.

The installed instrumentation includes the following:

- Station for solar and infrared radiation measurement, equipped with 6 pyranometers and 6 pyrgeometers, positioned to measure radiation in three orthogonal directions;
- Station for direct and diffuse radiation measurement, including high-precision instruments such as a pyrheliometer and a shaded pyranometer mounted on a solar tracker;
- Microclimatic station, measuring temperature, humidity, atmospheric pressure, wind speed, and wind direction;
- Photovoltaic monitoring system, involving a cloud interface for real-time visualization of the photovoltaic plant's production and consumption data.

3. Operation of the Plant

The operational functioning of the plant is structured into a set of interconnected processes, which, respectively, involve the following: energy conversion through the photovoltaic system and the conditioning of the generated electric power to meet the requirements of both load and electrolyser; hydrogen production; hydrogen purification; gas cooling and hydrogen reconversion into electricity through the fuel cell.

A detailed description of the involved processes is provided in the following sections.

3.1. Operational Configurations

The integrated system is designed to generate hydrogen via water electrolysis, primarily using the electrical energy produced by the photovoltaic system. However, if needed, it can also be powered directly by the electrical grid.

The operational flexibility of the system is ensured by its capability to be configured in different modes, in order to adapt its performance on the basis of either the availability of renewable energy or the purposes of the analysis, such as testing, calibration, or optimization of hydrogen production from photovoltaic sources. To this end, the plant can operate according to three distinct configurations, which differ mainly in the power supply modes for the electrolyser and auxiliary systems. They are referred to as: on-grid mode, stand-alone mode, and selective stand-alone mode.

Specifically, in on-grid mode (Figure 6), the power grid serves as a back-up supply. The power generated by the photovoltaic (PV) system is primarily used to feed all the main components of the system (electrolyser, fuel cell, cooling system, and other auxiliary systems), then to charge the battery (BSS). Any excess energy is exported to the grid, which,

in turn, supplies power when PV production is insufficient. This configuration is mainly used to test the plant at the electrolyser at full power.

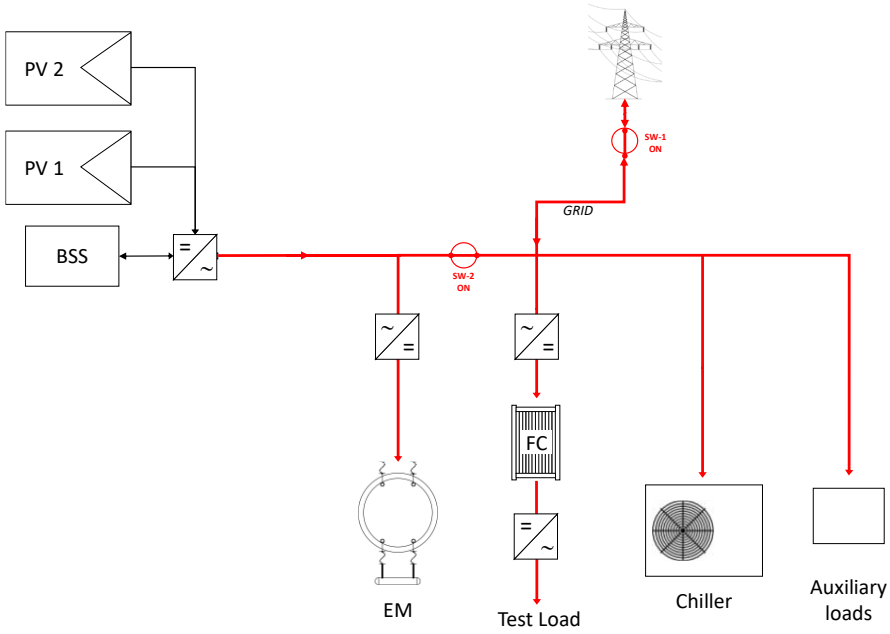

Figure 6. System on-grid configuration.

In the stand-alone mode (Figure 7), the plant operates independently of the power grid: the electrolyser, cooling system, and other auxiliary systems are powered exclusively by the photovoltaic array, with the support of the main battery storage systems (BSS). Under this configuration, the hydrogen produced is entirely derived from renewable sources.

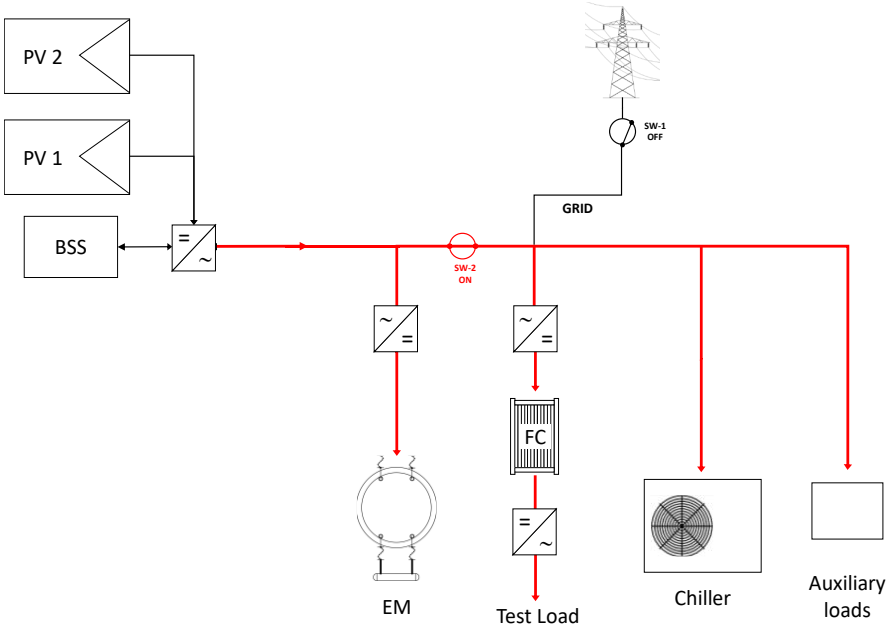

Figure 7. System stand-alone configuration.

In selective stand-alone mode (Figure 8), the electrolyser is powered by the photovoltaic array, while the cooling system and all the other auxiliary components are entirely powered by the electrical grid. This mode is used when renewable energy production is insufficient to meet the total system demand, and it is therefore allocated exclusively to the electrolyser to optimize hydrogen generation.

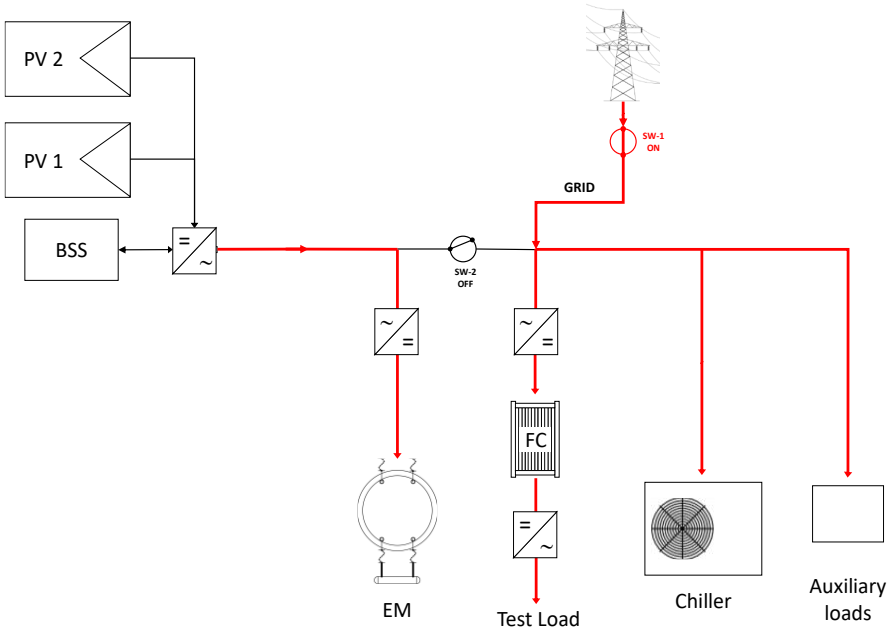

Figure 8. System selective stand-alone configuration.

A comparative summary of the three operational configurations, including key characteristics and performance considerations, is provided in Table 1 for clarity.

Table 1. System operational configurations.

Mode	Power Supply	PV System	Battery	Grid
On grid	PV + Battery + Grid	1. feeds all the components of the system 2. charges the battery 3. exports any excess energy to the grid	a. supplies power when PV production is insufficient b. is charged by the PV	a. delivers power when PV production + battery power supply is insufficient b. absorbs any surplus energy generated by the PV system
Stand-alone	PV + Battery	1. feeds all the components of the system 2. charges the battery	a. supplies power when PV production is insufficient b. is charged by the PV	not connected
Selective stand-alone	PV → Electrolyser Grid → Auxiliaries	1. feeds the electrolyser only 2. charges the battery	a. supplies power to the electrolyser when PV production is insufficient b. is charged by the PV	delivers power to all the auxiliary devices

3.2. Operational Phases

Hydrogen production, purification, and storage are carried out through a series of sequential operational phases, each characterized by a specific duration depending on the power supplied to the system. The sequence of phases that constitute a full operational cycle, from system start-up to shut-down, is outlined below:

- Start-up
- Initial inerting
- Standby

- Pre-start
- Purging
- Pressurization
- Production
- Depressurization
- Final inerting
- Shut-down

During the preliminary phase, the water supply line and hydrogen storage cylinder are opened. Subsequently, the cooling system is activated, and power switches are set according to the selected operating configuration (on-grid, stand-alone or selective stand-alone). At this point, the start-up phase can be triggered by pressing the corresponding button on the touchscreen of the Control Section panel.

The system then proceeds to the initial inerting phase, during which residual oxygen within the process line is purged by injecting nitrogen, supplied from a dedicated gas cylinder. Actually, this inerting phase plays a crucial role, as ambient air may infiltrate the process components while the system is not operating. Such infiltration could result in an accumulation of oxygen within the hydrogen processing section, creating hazardous conditions and increasing the risk of explosion.

The inerting phase consists of two successive stages. In fact, upon completion of the nitrogen pressurization step (Stage 1), the exhaust valves are automatically opened, and the system undergoes depressurization (Stage 2).

Once inerting is complete, the system enters standby mode, awaiting user input to initiate hydrogen production. By pressing a dedicated control button, the pre-start phase is activated, initiating electrolyte circulation within the electrolyser.

Following pre-start, the system automatically enters the purging phase, aimed at removing residual nitrogen from the system. During this phase, hydrogen and oxygen are generated and directed to their respective gas–liquid separators, then safely vented. Owing to nitrogen contamination, these gas streams cannot be utilized and are discarded.

Upon completion of purging, the system undergoes the pressurization phase, during which the control system gradually increases the current to the electrolyser until the user-defined setpoint is reached. Electrolysis generates hydrogen and oxygen, leading to a progressive pressure rise in the respective storage vessels.

Once a predetermined pressure threshold (currently about 12 bar) is reached, the system enters the production phase. From there, gas is sent to purification, the pressure continues to rise until it exceeds the delivery threshold of about 17.5 bar, at which point the back-pressure valve opens, allowing hydrogen to flow into the storage tank. The system pressure then slightly decreases and stabilizes under steady-state operating conditions.

Hydrogen production continues until either the standby or the stop command is activated via the PLC interface. The standby mode halts production and sets the system to an idle state. The stop command initiates the shutdown procedure, during which the power supply to the electrolyser is interrupted and the system enters the depressurization phase, so that gas lines are vented, and internal pressure is reduced to ambient pressure.

Following depressurization, the system executes the final inerting phase. As in the initial inerting, nitrogen is injected to displace residual hydrogen and oxygen, ensuring a safe and inert internal environment.

Once final inerting is complete, the system reverts to standby. At this point, full system shutdown can be performed by actuating the selector switch on the control cabinet. The shutdown sequence concludes with the closure of the nitrogen gas cylinder, the hydrogen storage cylinder, and the water supply valve.

The sequence of the operational phases can also be inferred from Figure 9, which depicts the flow diagram of the system's functioning scheme.

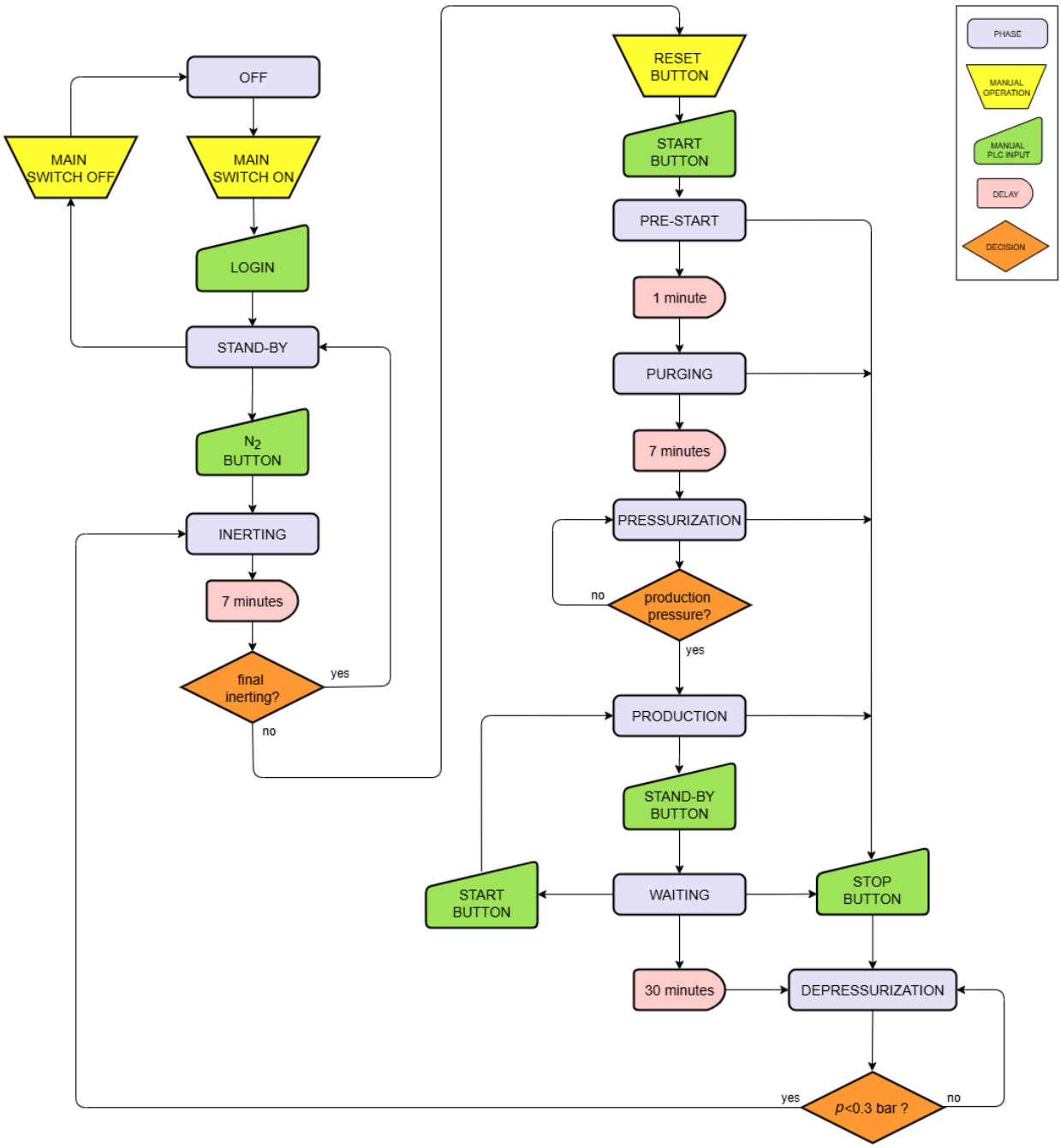

Figure 9. Process flow diagram.

4. Experimental Analysis

The experimental analysis was conducted to collect data suitable for evaluating the operational performance of the pilot system, with a view to supporting the future development of the research. The main objectives of this experimental phase were the following:

- To experimentally assess the main parameters of the process and energy flows.
- To analyze the relationship between these flows and the site's climatic conditions, with particular attention to solar radiation.
- To gather data useful for the future optimization of the system's operation.
- To obtain data for the subsequent calibration of system simulation models.

- Experimental activities were carried out by continuously monitoring the most significant parameters during the various operational phases of the hydrogen production system.

The system was tested under the two different operating configurations:

- On-grid configuration;
- selective stand-alone configuration.

Four experimental tests were conducted during different periods. The test conditions are specified in Table 2.

Table 2. Test Conditions.

Test	System Configuration	Objective/Focus
1	On-grid	To verify system performance under high input power conditions.
3	Selective stand-alone	To analyze the effect of the increase in power level feeding the electrolyser
4	Selective stand-alone	To evaluate the system's maximum continuous operating power when powered by the PV field
5	Selective stand-alone	To gather information on the duration of the initial and final inerting phases, purging, and depressurization

During these tests, several parameters were monitored. As far as the hydrogen production process is concerned, the registered parameters are the following: hydrogen pressure, oxygen concentration in the hydrogen stream, ambient temperature inside the container, as well as the voltage, current, and power delivered by the electrolyser (power set).

For the photovoltaic generator, PV production, output power from the inverter, and power to and from the battery were monitored. In addition, the following meteorological data were collected: air temperature and relative humidity, global horizontal irradiance (GHI), and its direct normal irradiance (DNI), and diffuse horizontal irradiance. The results of the measurements are detailed in the following sections.

5. Results

The section focuses on the key findings and outcomes of the study, highlighting the main observations and data trends obtained during the experimental phase. To pursue this goal and analyze system behaviour, some of the monitored parameters are reported and discussed in the following sub-sections.

5.1. Test 1

During Test 1 the system was set in on-grid mode. The objective of this test was to verify the system's performance under elevated electrolyser operating regimes.

Figures 10 and 11 show the time trend of air temperature, relative humidity, and solar irradiance during the test, whereas PV production is reported in Figure 12.

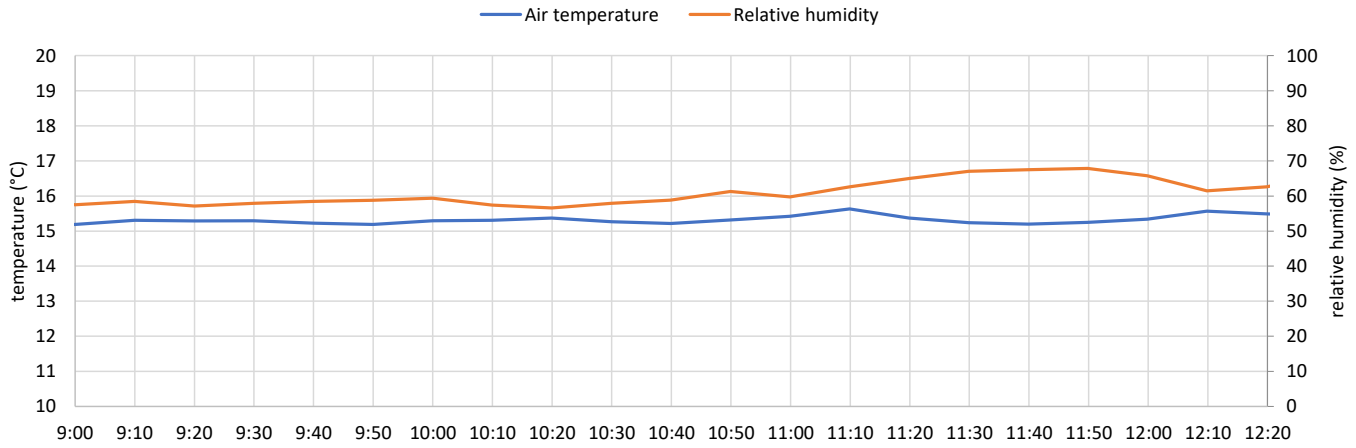

Figure 10. Air temperature and Relative humidity—Test 1.

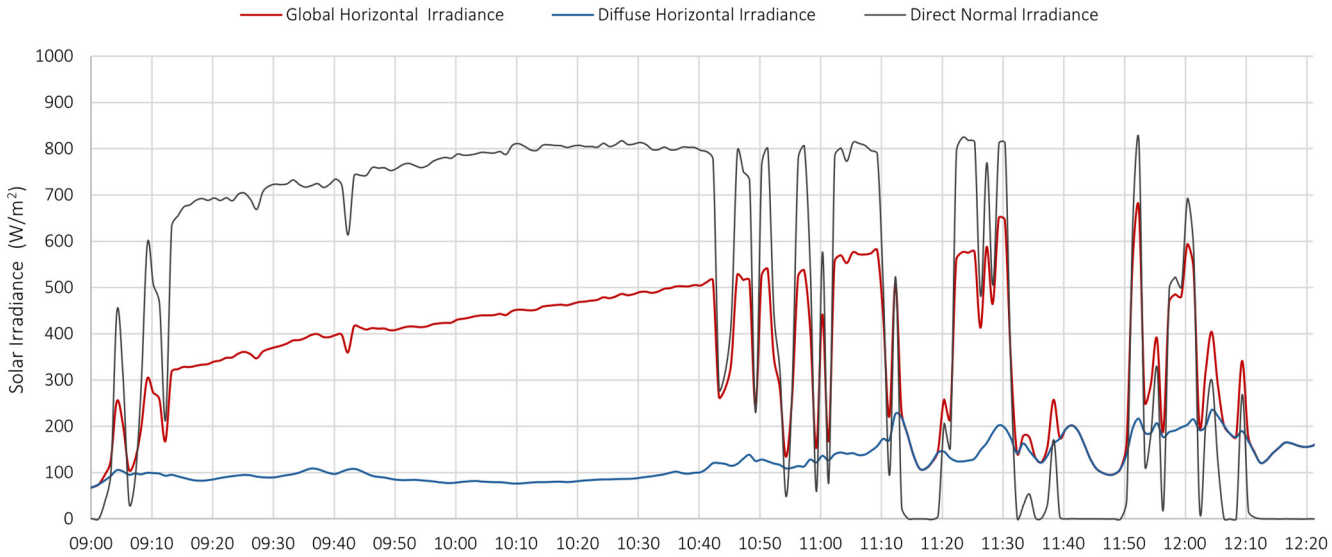

Figure 11. Solar radiation—Test 1.

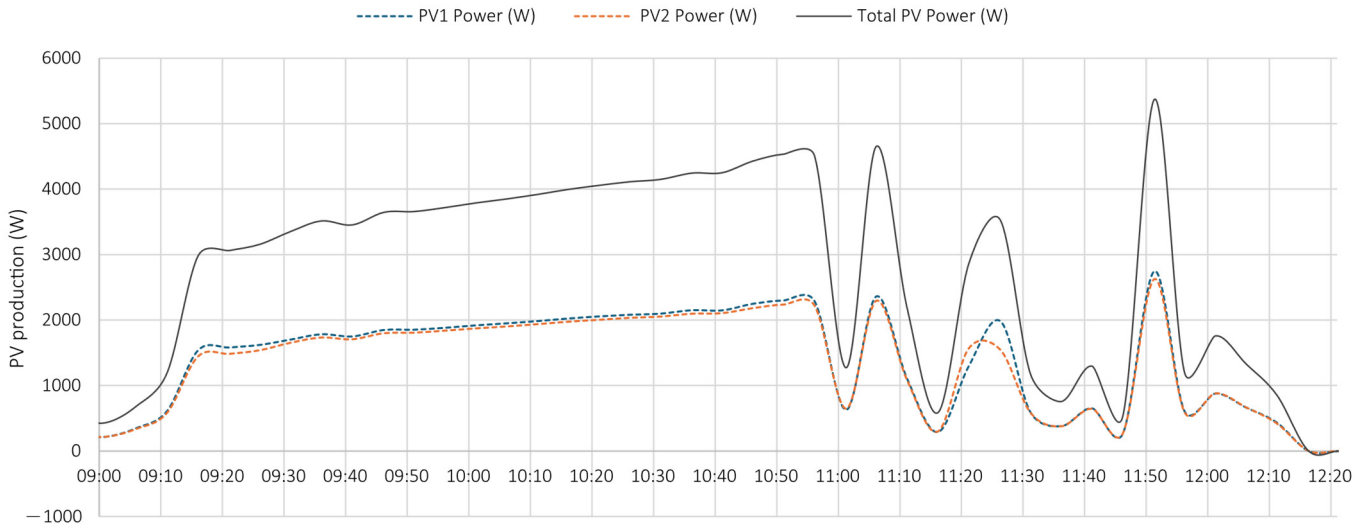

Figure 12. PV production—Test 1.

The operational conditions of the test are detailed in Table 3, which also highlights the power set.

Table 3. Test 1 Operational phases.

Phase		Start	End	Power Set (%)
INERTIZATION	Stage 1	9:53	9:57	
	Stage 2	9:57	10:04	
STANDBY		10:04	10:06	
PRE-START		10:06	10:07	20
PURGING		10:07	10:14	20
PRESSURIZATION		10:14	10:22	20
		10:22	10:32	50
		10:32	11:14	75
PRODUCTION		11:14	11:45	75
DEPRESSURIZATION		11:45	11:59	
INERTIZATION	Stage 1	11:59	12:03	
	Stage 2	12:03	12:08	

The power demand during the test (9:53–12:08) can be inferred from the trends shown in Figure 13, which illustrates the electric power flows from the photovoltaic system, the grid, and the battery. Negative values of the grid and battery power flows indicate that energy is supplied to the system (i.e., battery discharge or power drawn from the grid), while positive values imply that energy is absorbed by these components (i.e., battery charging or surplus PV power being stored).

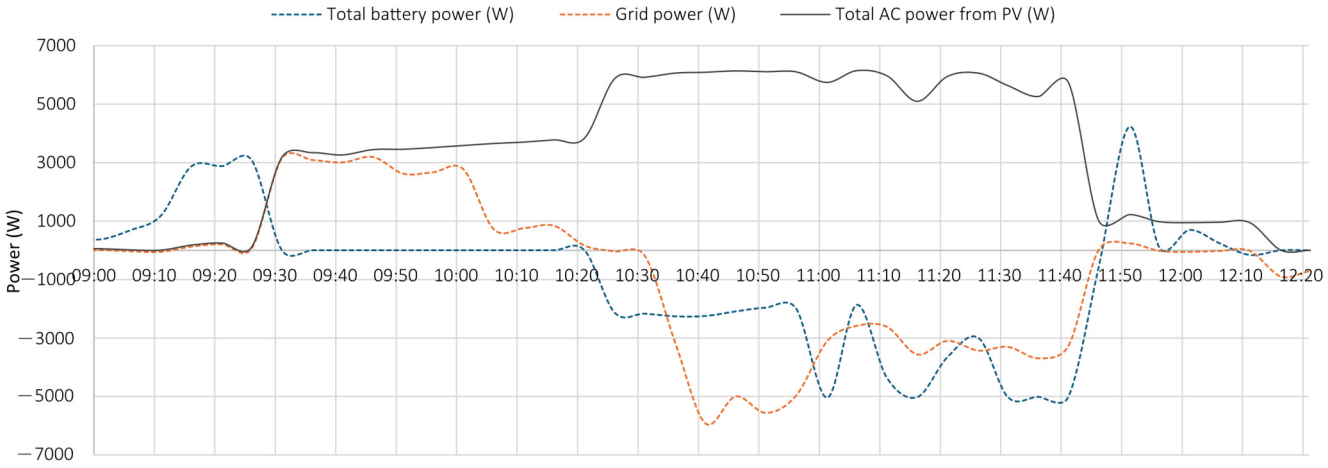

Figure 13. Electric power flows: PV AC output, grid exchange, and battery operation—Test 1.

Between 10:30 and 11:45, the power setpoint of the electrolyser was held at 75% (Table 3), corresponding to a significant increase in power demand. This demand was met through a combined contribution from the PV system, the battery, and the grid. Specifically, during this interval

- the PV system operated near its peak output, delivering power to the load;
- the battery supplied additional power, as indicated by the negative values of the dashed blue curve, representing battery discharge;
- the grid also provided power, as demonstrated by the negative portion of the orange curve, particularly during the initial phase.

This simultaneous contribution from all three sources highlights the coordinated operation of the hybrid system to meet the high consumption required by the 75% power setpoint of the electrolyser.

The energy demand of the system is also inferable from Figure 14: the electrolyser (power set 75%) and all the needed equipment account for about 14 kW.

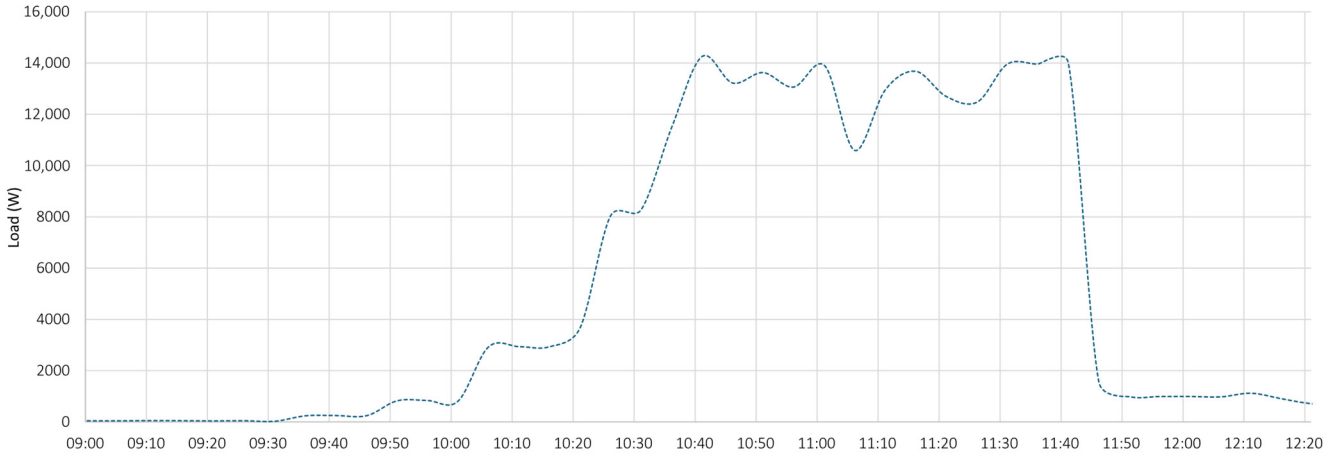

Figure 14. Time trend of the total load—Test 1.

Figure 15 shows the time evolution of hydrogen pressure and electrolyser power setpoint across the various operational phases of the test.

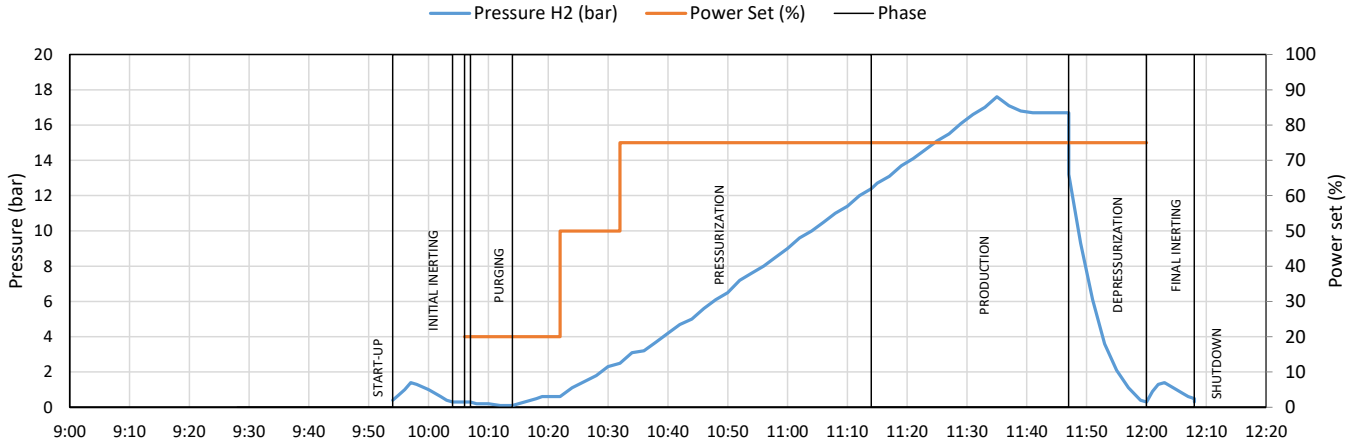

Figure 15. Temporal evolution of hydrogen pressure and power set—Test 1.

Following system startup and the initial inerting phase, the power set was gradually increased, causing a corresponding rise in the hydrogen pressure time gradient. Around 11:30, a plateau in pressure was observed, indicating the start of hydrogen delivery to the storage tank. Shortly after, the system was stopped, so that it entered the depressurization phase, during which the pressure rapidly decreased, followed by final inerting and transition to standby. The vertical black lines indicate key phase changes, providing reference points for interpreting system behaviour over time.

The key values of selected parameters (initial and final pressure, duration and pressure gradient) corresponding to the different phases of the process are detailed in Table 4.

Table 4. Test 1 Operational parameters.

Phase		Initial Pressure (bar)	Final Pressure (bar)	Duration (min)	Dp/Dt (bar/min)
INERTIZATION	Stage 1	0.3	1.4	4	1.1
	Stage 2	1.4	0.3	7	−1.1
STANDBY		0.3	0.3	2	0.0
PRE-START		0.3	0.3	1	0.0
PURGING		0.3	0.1	7	−0.2
PRESSURIZATION		0.3	0.6	8	0.3
		0.6	2.5	10	1.9
		2.5	12.4	42	9.9
PRODUCTION		12.4	16.7	31	4.3
DEPRESSURIZATION		16.7	0.3	14	−16.4
INERTIZATION	Stage 1	0.3	1.4	4	1.1
	Stage 2	1.4	0.3	5	−1.1

5.2. Test 2

Test 2 represents a preliminary evaluation of the selective stand-alone configuration. During the test, the power supplied to the electrolyser was gradually increased up to 35% of the maximum power setpoint.

After a brief production period at this last power level, the system unexpectedly shut down: the depressurization sequence was automatically triggered, followed by the inerting phase and a complete stop of the process. This behaviour might be associated with transient instability in the AC power supply delivered by the inverter in selective stand-alone mode. Such instability, potentially due to voltage sag caused by rapid and strong load variations, may have exceeded the inverter's response capabilities at a power demand of the electrolyser (≈3.5 kW) quite close to the maximum power of the inverter.

These conditions could have been interpreted by the control system as a potential safety risk, triggering the internal protection logic and initiating a fail-safe shutdown procedure. Although further investigation is required, particularly through a detailed analysis of voltage profiles, this hypothesis is supported by the activation of the system's safety relay, as recorded in the PLC log.

On the other hand, in the literature [34–37], this specific issue has been already revealed, especially in weak microgrids operated in the stand-alone mode. In fact, in such a case, grid instability phenomena often occur, especially when no rotating generators (synchronous generator) are used to support conventional current-source inverters or when the number of the latter on the grid increase significantly. For this reason, currently, last generation inverters and control methods are being designed, developed, and tested and they seem to have the capability to cope with the grid instability issue, thanks to their abilities to control the rms value and the frequency of their output voltage in a way similar to that implemented in the presence of synchronous generators. In practice, this seems possible thanks to their ability of emulating the inertia of synchronous generators, by supplying high-speed transient controlled currents. That said, it will be very interesting to investigate in more depth the aforementioned phenomenon in future, by taking advantage, for our pilot plant, of a last generation control method on an inverter with higher rated power. Despite this unexpected interruption, Test 2 provided in any case valuable insights into the pressurization and depressurization processes, as well as the associated pressure gradients.

The operational conditions of the test are detailed in Table 5, which also highlights the power set.

Table 5. Test 2 Operational phases.

Phase		Start	End	Power Set (%)
INERTIZATION	Stage 1	11:27	11:29	
	Stage 2	11:36	11:38	
STANDBY		11:36	11:38	
PRE-START		11:38	11:39	20
PURGING		11:39	11:46	20
PRESSURIZATION		11:46	11:51	20
		11:51	12:22	30
		12:22	12:35	35
DEPRESSURIZATION		12:35	12:43	
INERTIZATION	Stage 1	12:43	12:47	
	Stage 2	12:47	12:52	

Figures 16 and 17 show the time trend of air temperature, relative humidity, and solar irradiance recorded during the test, whereas Figure 18 illustrates the PV production.

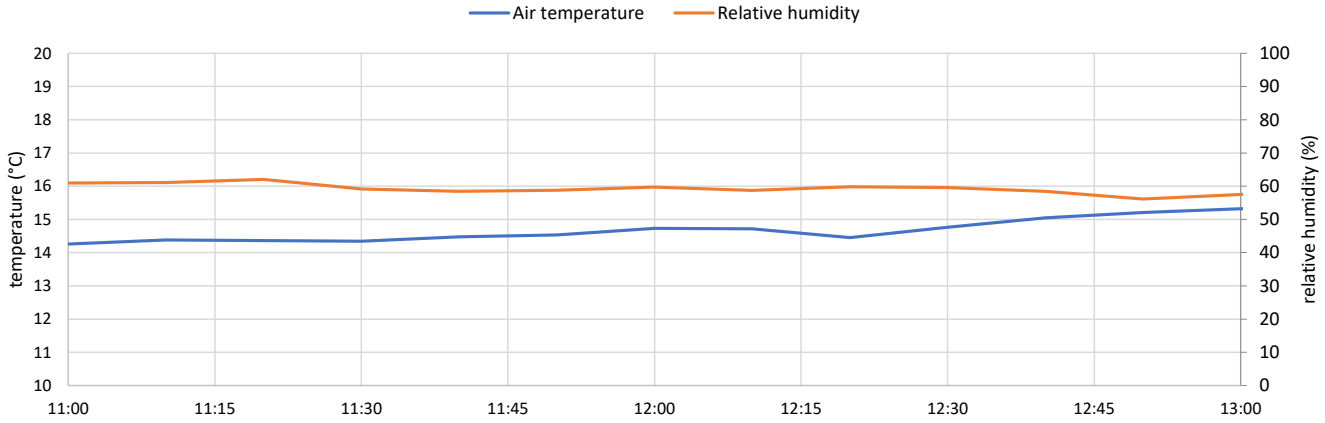

Figure 16. Air temperature and Relative humidity—Test 2.

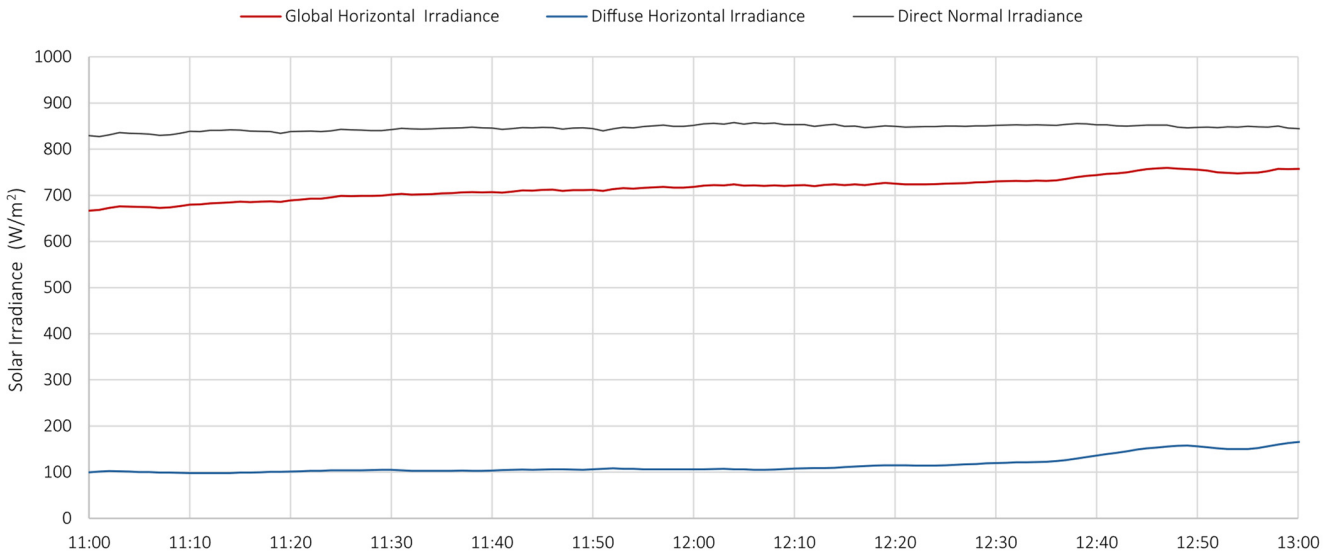

Figure 17. Solar radiation—Test 2.

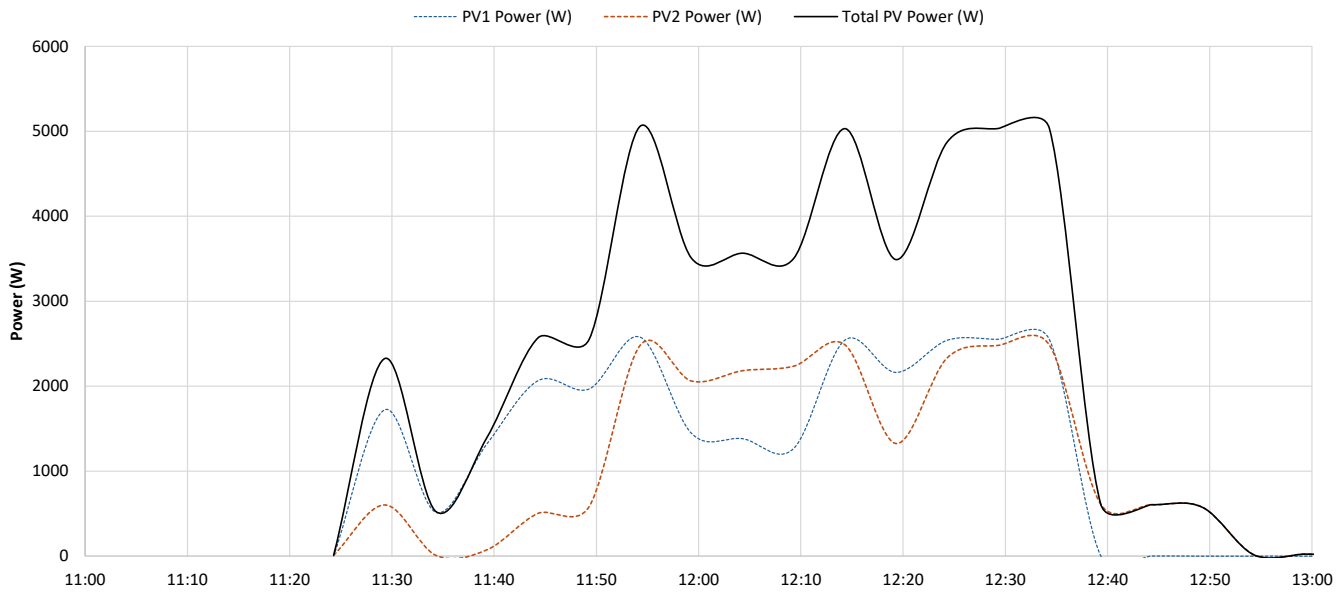

Figure 18. PV production—Test 2.

It is worth noting that, in this case, PV production was limited by the load demand, as in selective stand-alone mode the inverter operates off-grid and therefore cannot transfer any surplus energy to the electrical grid.

This behaviour is also inferable from the analysis of the electric power flows shown in Figure 19, where the black line, referred to as inverter power, represents the apparent power delivered by the inverter in selective stand-alone mode, which reflects the load demand. In this configuration, the demand is generated only by the electrolyser, whereas all the auxiliary devices are fed by the grid.

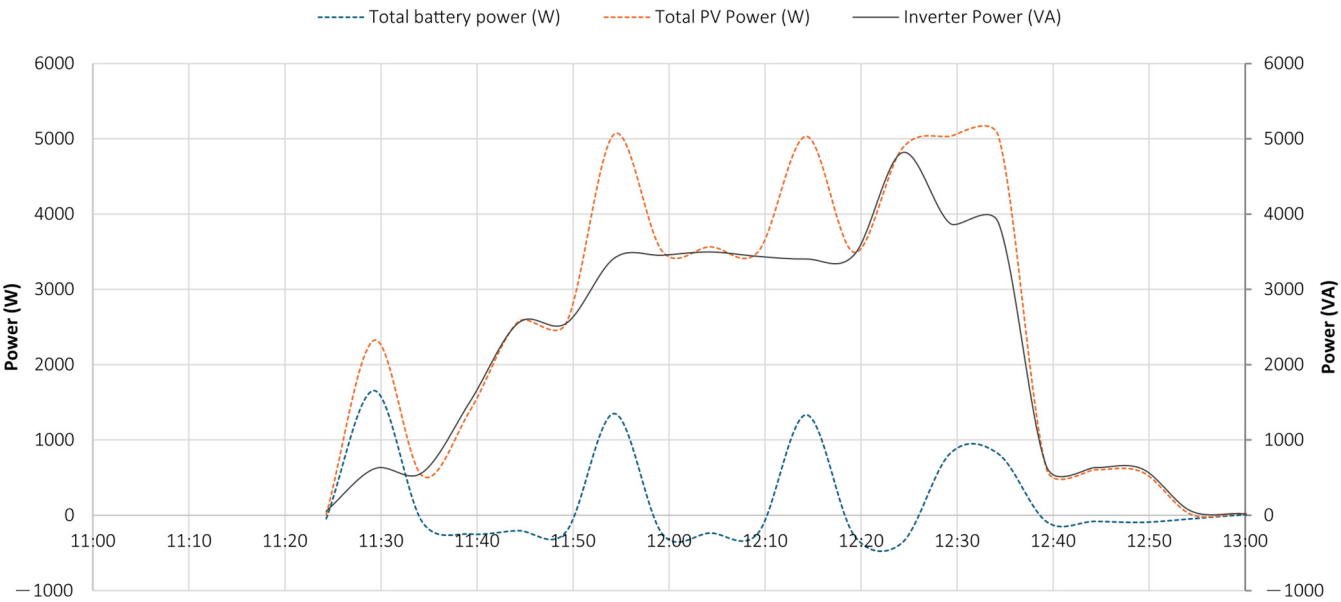

Figure 19. Electric power flows: PV production, inverter output, and battery operation—Test 2.

Figure 20 shows the time evolution of hydrogen pressure and the electrolyser power setpoint across the various operational phases of the test.

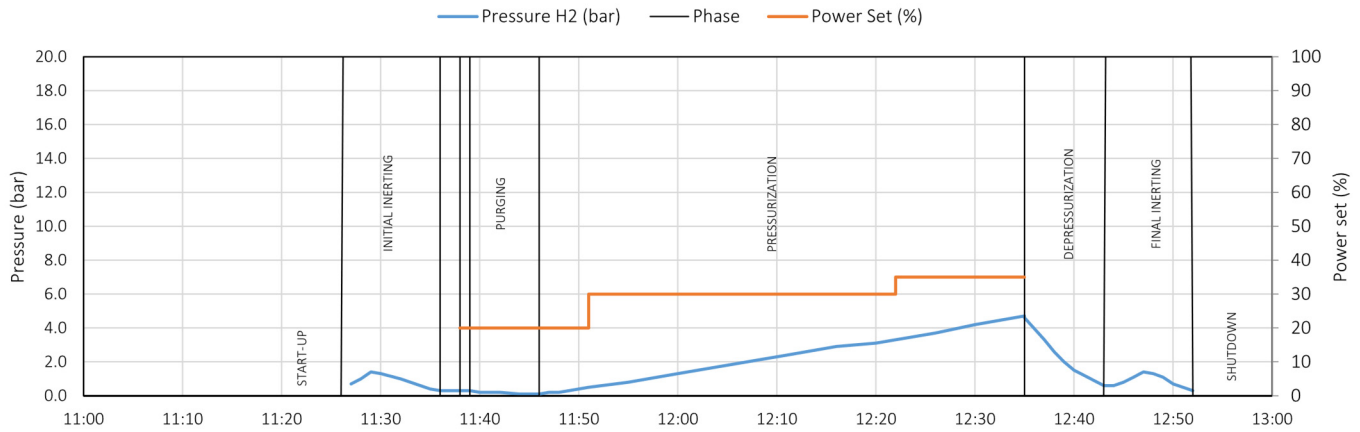

Figure 20. Temporal evolution of hydrogen pressure and power set—Test 2.

The key values of selected parameters (initial and final pressure, duration and pressure gradient) corresponding to the different phases of the process are detailed in Table 6.

Table 6. Test 2 Operational parameters.

Phase		Initial Pressure (bar)	Final Pressure (bar)	Duration (min)	Dp/Dt (bar/min)
INERTIZATION	Stage 1	0.7	1.4	2	0.7
	Stage 2	1.4	0.3	2	−1.1
STANDBY		0.3	0.3	2	0.0
PRE-START		0.3	0.3	1	0.0
PURGING		0.3	0.1	7	−0.2
PRESSURIZATION		0.1	0.5	5	0.4
		0.5	3.3	31	2.8
		3.3	4.7	13	1.4
DEPRESSURIZATION		4.6	0.6	8	−4.0
INERTIZATION	Stage 1	0.6	1.4	4	0.8
	Stage 2	1.4	0.3	5	−1.1

5.3. Test 3

Test 3 pertains to the measurements conducted under the selective stand-alone configuration. The objective of the test was to assess the maximum power level at which the system could operate continuously, relying exclusively on the photovoltaic field for power supply.

Following system start-up, the power setpoint (Power Set) was gradually increased up to 35%. Under these conditions, however, as occurred during Test 2, the system did not reach the production phase: after approximately one hour of pressurization, the internal protection logic was triggered, leading to system depressurization and a transition to standby mode. Subsequently, the system was promptly restarted with the power setpoint reduced to 30%. In this configuration, stable operation was achieved, and the system successfully entered the production phase.

The operational conditions of the test are detailed in Table 7, which also highlights the power set.

Table 7. Test 3 Operational phases.

Phase		Start	End	Power Set (%)
INERTIZATION	Stage 1	8:38	8:40	
	Stage 2	8:40	8:43	
STANDBY		8:43	8:45	
PRE-START		8:45	8:46	20
PURGING		8:46	8:53	20
PRESSURIZATION		8:53	8:56	20
		8:56	8:58	25
		8:58	9:00	30
		9:00	10:03	35
DEPRESSURIZATION		10:03	10:19	
INERTIZATION	Stage 1	10:19	10:22	
	Stage 2	10:22	10:27	
STANDBY		10:27	10:28	
PRE-START		10:28	10:29	
PURGING		10:29	10:36	
PRESSURIZATION		10:36	10:37	20
		10:37	13:03	30
PRODUCTION		13:03	13:10	30
DEPRESSURIZATION		13:10	13:25	
INERTIZATION	Stage 1	13:25	13:29	
	Stage 2	13:29	13:33	

Figures 21 and 22 show the time trend of air temperature, relative humidity and solar irradiance recorded during the test, whereas Figure 23 illustrates the PV production.

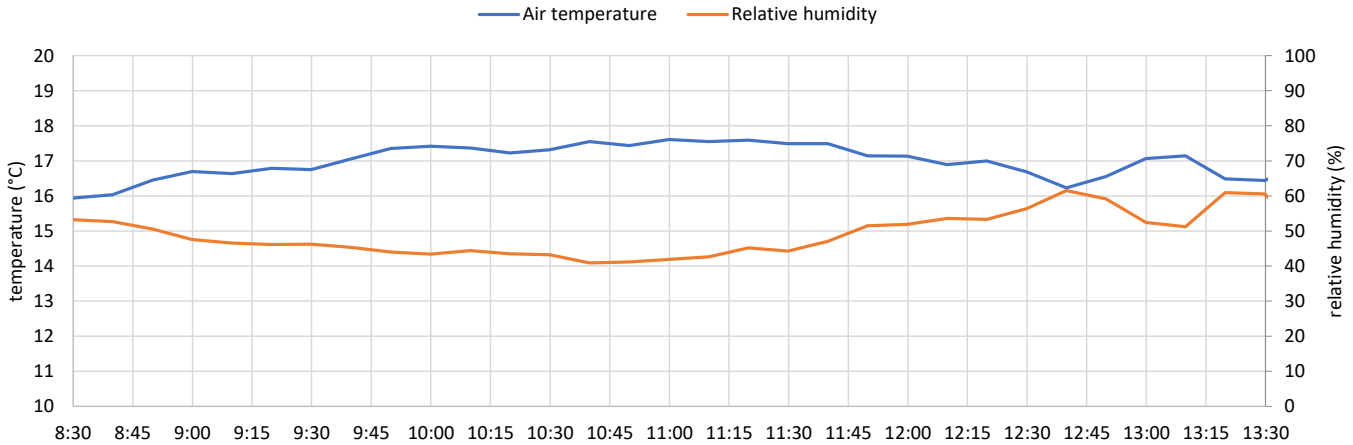

Figure 21. Air temperature and Relative humidity—Test 3.

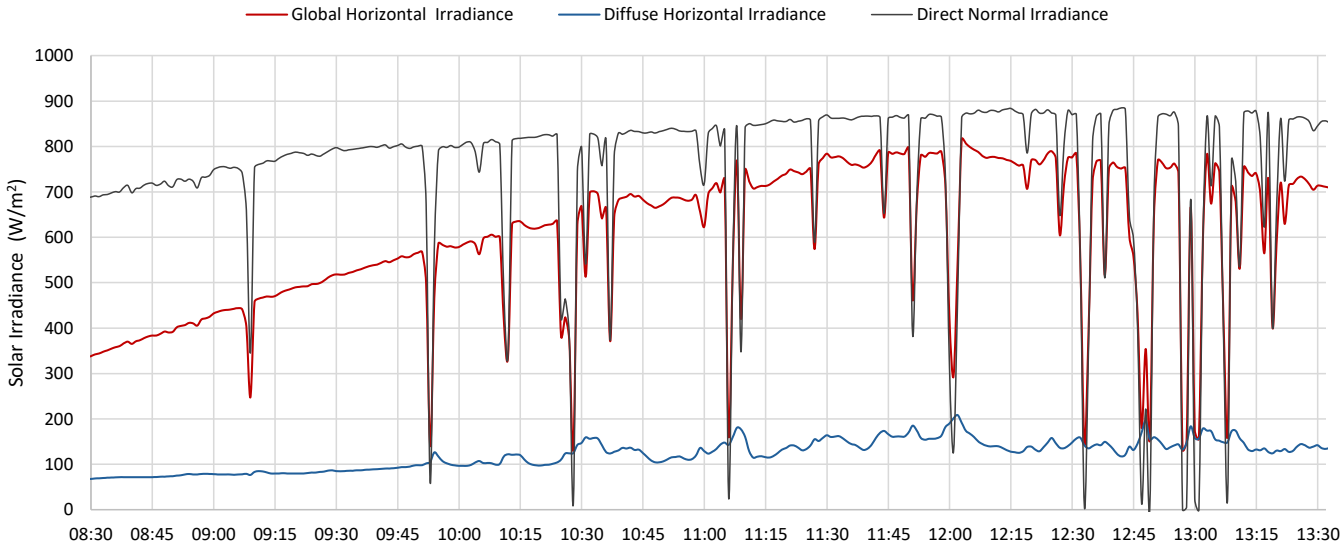

Figure 22. Solar radiation—Test 3.

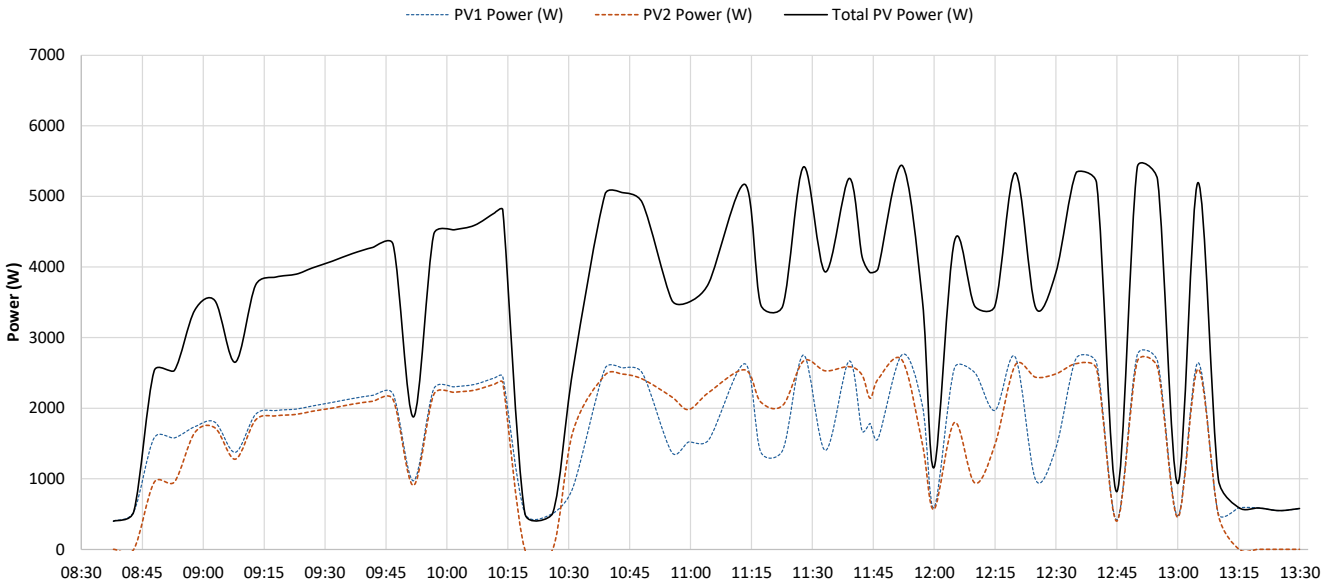

Figure 23. PV production—Test 3.

Similarly to the analysis performed for Test 2, Figure 24 shows the electric power flows, while Figure 25 depicts the time evolution of hydrogen pressure and the electrolyser power setpoint across the various operational phases of the test.

The key values of selected parameters (initial and final pressure, duration and pressure gradient) corresponding to the different phases of the process are detailed in Table 8.

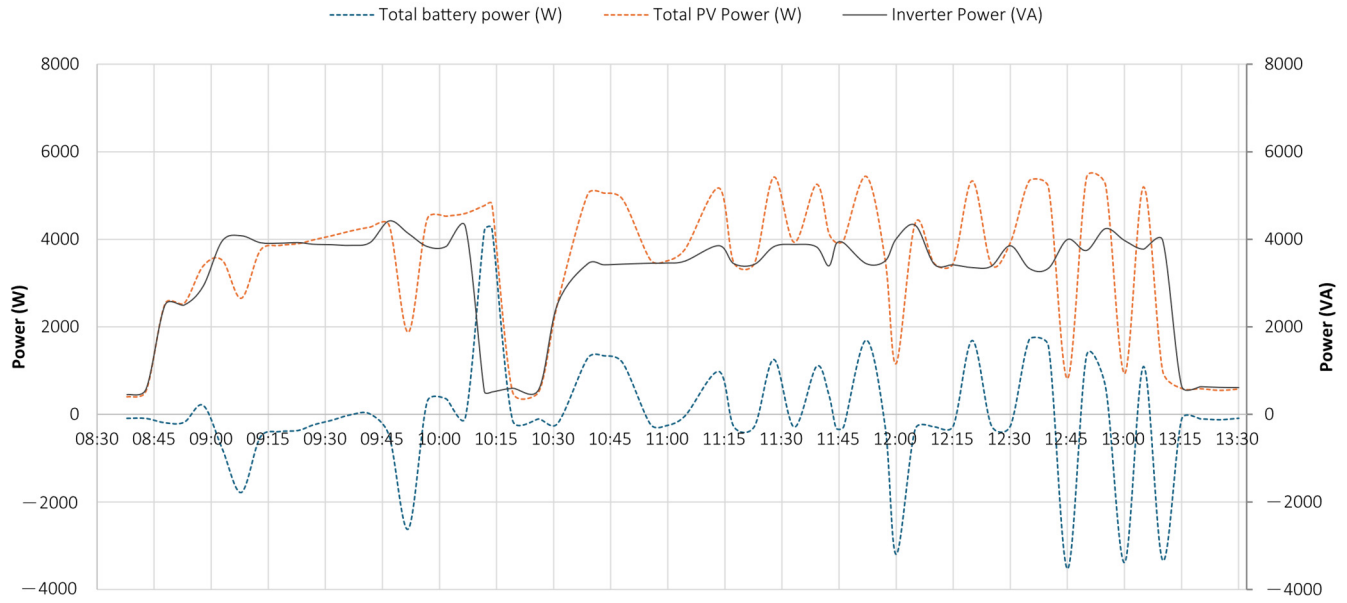

Figure 24. Electric power flows: PV production, inverter output, and battery operation—Test 3.

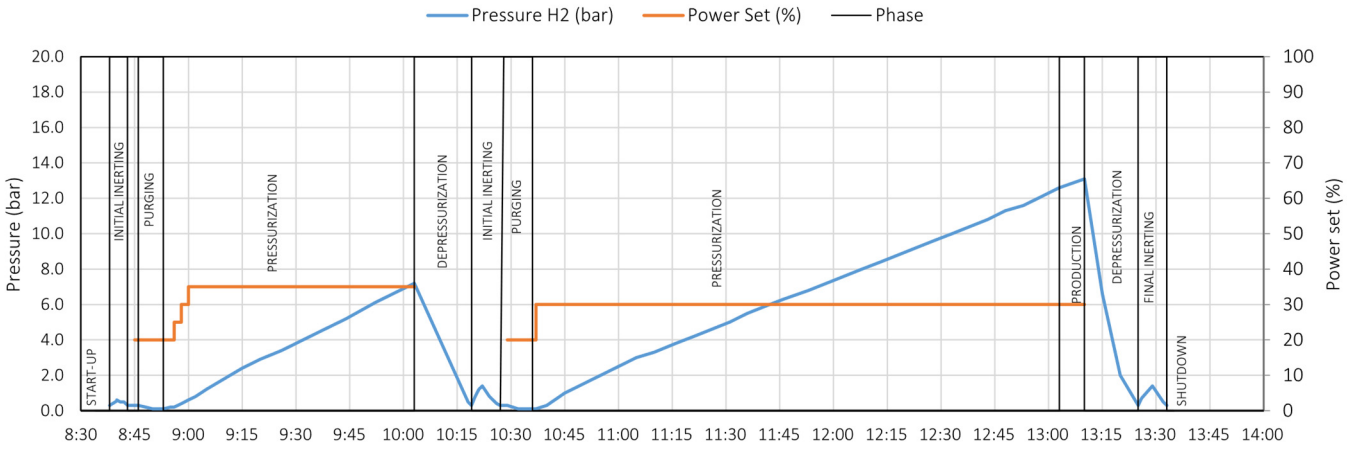

Figure 25. Temporal evolution of hydrogen pressure and power set—Test 3.

Table 8. Test 3 Operational parameters.

Phase		Initial Pressure (bar)	Final Pressure (bar)	Duration (min)	Dp/Dt (bar/min)
INERTIZATION	Stage 1	0.3	0.6	2	0.3
	Stage 2	0.6	0.3	3	−0.3
STANDBY		0.3	0.3	2	0.0
PRE-START		0.3	0.3	1	0.0
PURGING		0.3	0.1	6	−0.2
PRESSURIZATION		0.1	0.2	3	0.1
		0.2	0.4	2	0.2
		0.4	0.6	2	0.2
DEPRESSURIZATION		0.6	7.2	63	6.6

Table 8. *Cont.*

Phase		Initial Pressure (bar)	Final Pressure (bar)	Duration (min)	Dp/Dt (bar/min)
INERTIZATION	Stage 1	7.2	0.3	16	−6.9
	Stage 2	0.3	1.4	3	1.1
STANDBY		1.4	0.3	5	−1.1
PRE-START		0.3	0.3	1	0.0
PURGING		0.3	0.3	1	0.0
PRESSURIZATION		0.3	0.1	7	−0.2
		0.1	0.1	1	0.0
PRODUCTION		0.1	12.6	146	12.5
DEPRESSURIZATION		12.6	13.1	7	0.5
INERTIZATION	Stage 1	13.1	0.3	15	−12.8
	Stage 2	0.3	1.4	4	1.1

5.4. Test 4

Test 4 refers to the data collected in the selective stand-alone configuration. The objective of this measurement was to obtain additional information on the durations of the initial and final inerting phases, purging, and depressurization.

Figures 26 and 27 show the time trend of air temperature, relative humidity, and solar irradiance recorded during the test, whereas Figure 28 illustrates the PV production. The operational conditions of the test are detailed in Table 9, which also highlights the power set.

Similarly to the analysis performed for the other tests, Figure 29 shows the electric power flows, while Figure 30 depicts the time evolution of hydrogen pressure and electrolyser power setpoint across the various operational phases of the test.

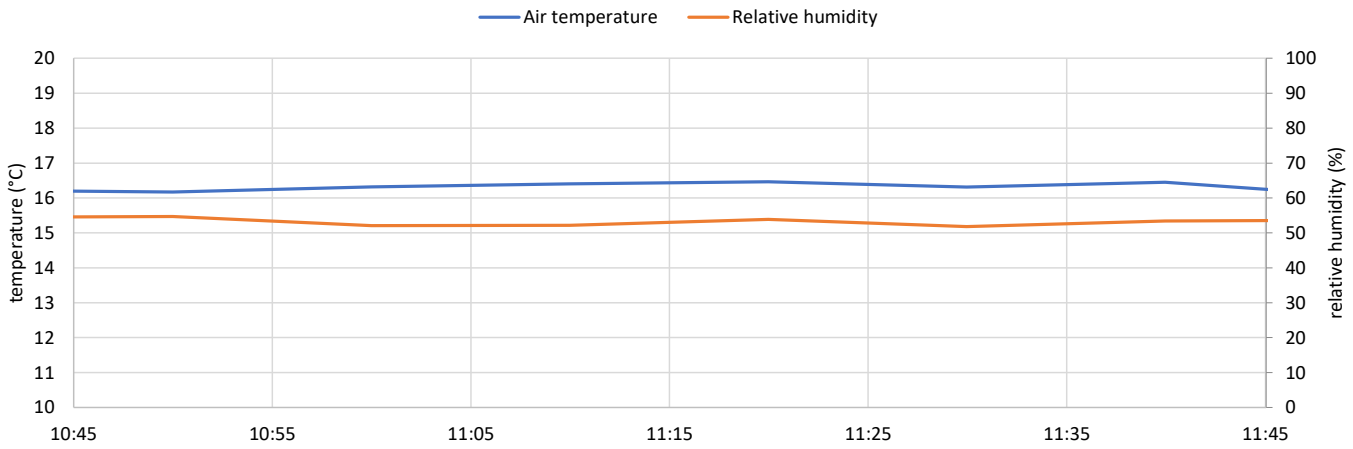

Figure 26. Air temperature and Relative humidity—Test 4.

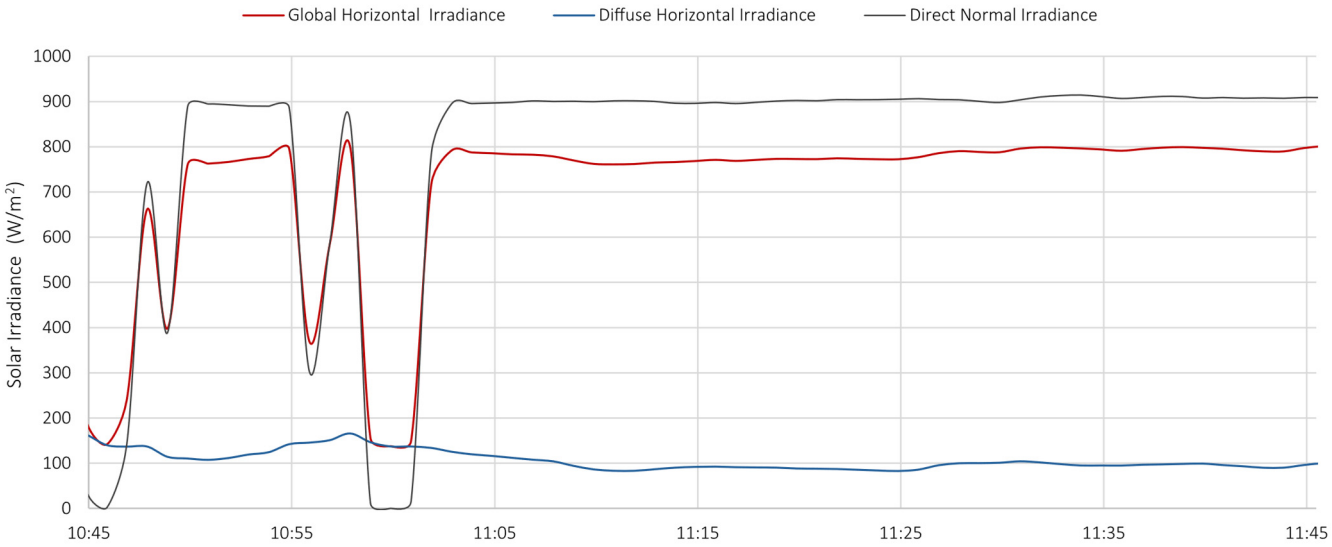

Figure 27. Solar radiation—Test 4.

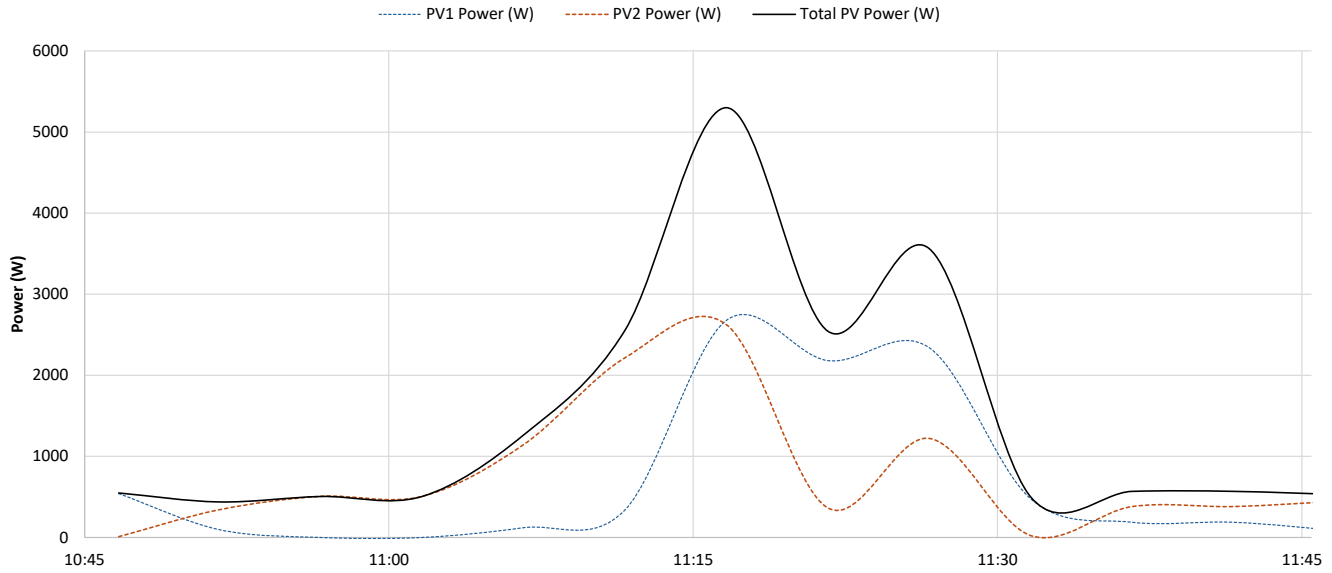

Figure 28. PV production—Test 4.

Table 9. Test 4 operational phases.

Phase		Start	End	Power Set (%)
INERTIZATION	Stage 1	10:53	10:55	
	Stage 2	10:57	11:02	
STANDBY		11:02	11:06	
PRE-START		11:06	11:07	
PURGING		11:07	11:13	20
PRESSURIZATION		11:13	11:24	20
		11:24	11:33	30
DEPRESSURIZATION		11:33	11:36	
INERTIZATION	Stage 1	11:36	11:39	
	Stage 2	11:39	11:43	

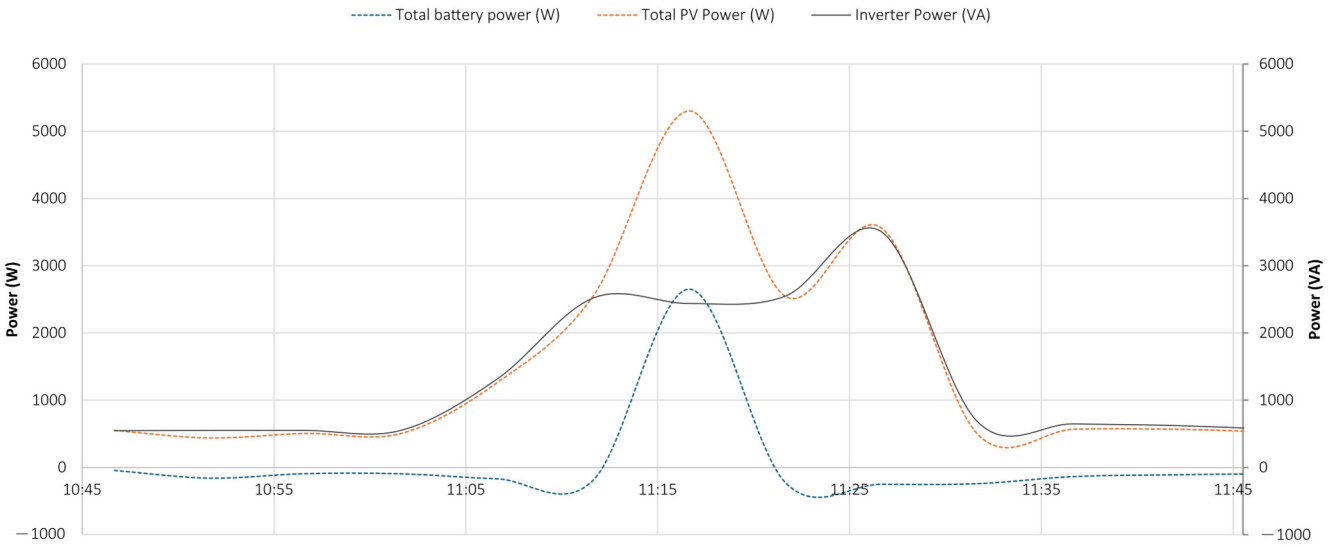

Figure 29. Electric power flows: PV production, inverter output, and battery operation—Test 4.

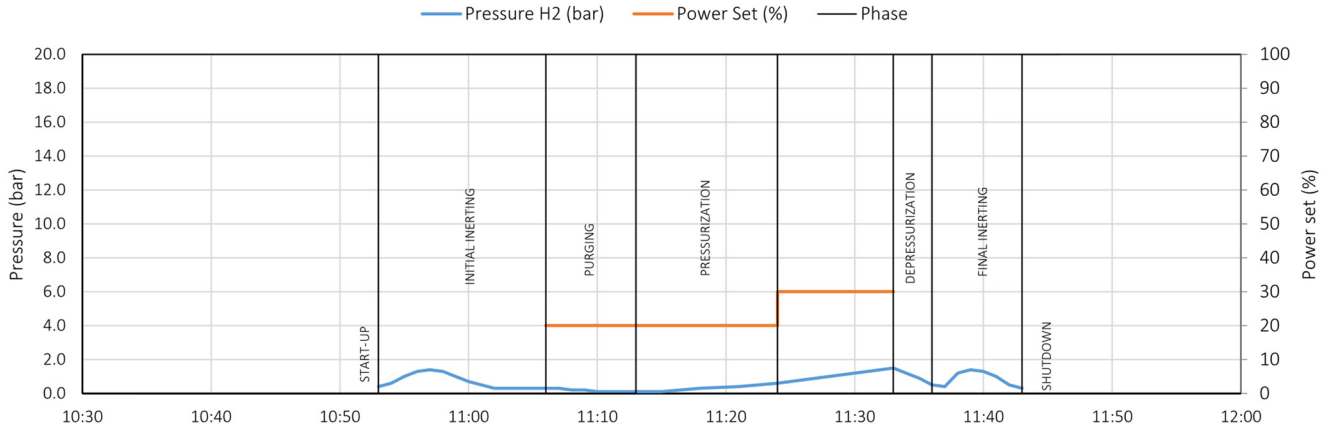

Figure 30. Temporal evolution of hydrogen pressure and power set—Test 4.

The key values of selected parameters (initial and final pressure, duration, and pressure gradient) corresponding to the different phases of the process are detailed in Table 10.

Table 10. Test 4 operational parameters.

Phase		Initial Pressure (bar)	Final Pressure (bar)	Duration (min)	Dp/Dt (bar/min)
INERTIZATION	Stage 1	0.4	1.4	4	1.0
	Stage 2	1.4	0.3	5	−1.1
STANDBY		0.3	0.3	4	0.0
PRE-START		0.3	0.3	1	0.0
PURGING		0.3	0.1	6	−0.2
PRESSURIZATION		0.1	0.6	11	0.5
		0.6	1.5	11	0.9
DEPRESSURIZATION		1.5	0.5	3	−1.0
INERTIZATION	Stage 1	0.5	1.4	3	0.9
	Stage 2	1.4	0.3	4	−1.1

6. Discussion

The analysis of the experimental results enabled a detailed examination of the system's behaviour across the various operational phases, allowing the identification of possible inefficiencies or faults. More importantly, it provided a valuable dataset for the development and calibration of system simulation models. In fact, the availability of simulation models is essential for evaluating the system's performance under different climatic conditions or load configurations, thus underpinning scalability analysis.

Below are summarized data describing the system's behaviour during the various process phases. For each phase, the average duration and the pressure increase trend over time within the system are reported.

6.1. Initial Inerting Phase

The initial inertization phase had an average total duration of about 7 min, with an initial pressurization stage lasting approximately 3 min and a depressurization stage lasting 4 min. During the first stage the pressure increases, while in the second stage it decreases with the rate reported in Table 11.

Table 11. Initial inerting phase.

Test	Duration (min)	Initial Pressure p_i (bar)	Final Pressure p_f (bar)	$\Delta p/\Delta t$ (bar/min)
Stage 1				
1	4	0.3	1.4	0.275
2	2	0.3	1.4	0.550
3a	2	0.3	1.4	0.550
3b	3	0.3	1.4	0.300
4	4	0.3	1.4	0.275
average	3.0			0.413
Stage 2				
1	7	1.4	0.3	−0.157
2	2	1.4	0.3	−0.550
3a	3	1.4	0.3	−0.367
3b	5	1.4	0.3	−0.220
4	5	1.4	0.3	−0.220
average	4.3			−0.324

6.2. Pre-Start Phase

The duration of the pre-start phase was consistent across all measurements, remaining constant at 1 min. During this phase, no pressure increase was recorded within the system.

6.3. Purging Phase

The average duration of the purging phase was 6.5 min. The initial and final pressures were found to be the same across all measurements (Table 12).

Table 12. Purging phase.

Test	Duration (min)	Initial Pressure p_i (bar)	Final Pressure p_f (bar)	$\Delta p/\Delta t$ (bar/min)
1	7	0.3	0.1	−0.029
2	7	0.3	0.1	−0.029
3a	7	0.3	0.1	−0.029
3b	7	0.3	0.1	−0.029
4	6	0.3	0.1	−0.033
average	6.5			−0.031

6.4. Pressurization Phase

With regard to the pressurization phase, the data obtained are categorized based on the power set (Table 13). In this context, it is worth highlighting the pivotal role played by the pressure increase rate within the system over time in relation to the selected power set, as this parameter allows for the estimation of the time required for complete pressurization.

Table 13. Pressurization phase.

Test	Duration (min)	Initial Pressure p_i (bar)	Final Pressure p_f (bar)	$\Delta p/\Delta t$ (bar/min)
Power set 20%				
1	8	0.3	0.6	0.038
2	5	0.3	0.5	0.040
3a	3	0.1	0.2	0.033
3b	1	0.1	0.1	0.000
4	11	0.1	0.6	0.045
Average	5.6			0.031
Power set 30%				
2	31	0.5	3.3	0.090
3a	2	0.4	0.6	0.100
3b	146	0.1	12.6	0.086
4	11	0.6	1.5	0.082
Average	47.5			0.089
Power set 35%				
2	13	3.3	4.7	0.108
3a	63	0.6	7.2	0.105
Average	41.2			0.101
Power set 50%				
1	10	0.6	2.5	0.190
Power set 75%				
1	42	2.5	12.4	0.236

6.5. Depressurization Phase

Similar considerations to those made for the pressurization phase can be applied to the depressurization phase. In this case as well, the phase duration depends on when the user decides to initiate the system shutdown. However, important insights can be gained

from the pressure reduction rate, which is useful for simulating the total shutdown time of the plant (Table 14).

Table 14. Depressurization phase.

Test	Duration (min)	Initial Pressure p_i (bar)	Final Pressure p_f (bar)	$\Delta p/\Delta t$ (bar/min)
1	14	16.7	0.3	−1.171
2	8	4.6	0.6	−0.500
3a	16	7.2	0.3	−0.431
3b	15	13.1	0.3	−0.853
4	3	1.5	0.5	−0.333
average	11.2			−0.658

Furthermore, the analysis of the depressurization process is crucial to verify the system performance from the safety point of view.

In particular, the rapid depressurization observed in Test 1 (up to 16.4 bar/min) demonstrates the system's capability to handle shutdown procedures safely and return to ambient conditions within a short timeframe.

These results confirm that the system remains operationally stable and reliably executes emergency protocols, even under simulated scenarios of abrupt production interruption.

6.6. Final Inerting Phase

Finally, regarding the final inerting phase, its average total duration was approximately 8 min, with an initial pressurization stage lasting 3.6 min and a depressurization stage lasting 4.6 min. During the first stage the pressure increases, while in the second stage it decreases with the rate reported in Table 15.

Table 15. Final inerting phase.

Test	Duration (min)	Initial Pressure p_i (bar)	Final Pressure p_f (bar)	$\Delta p/\Delta t$ (bar/min)
Stage 1				
1	4	0.3	1.4	0.275
2	4	0.3	1.4	0.275
3a	3	0.3	1.4	0.367
3b	4	0.3	1.4	0.275
4	3	0.5	1.4	0.300
average	3.6			0.298
Stage 2				
1	5	1.4	0.3	−0.220
2	5	1.4	0.3	−0.220
3a	5	1.4	0.3	
3b	4	1.4	0.3	−0.275
4	4	1.4	0.3	−0.275
average	4.6			−0.248

6.7. Correlations Between Data

Since the internal pressure of the system is one of the key parameters for assessing hydrogen production, a regression analysis was carried out to identify a relationship regarding the pressure trend over time. The analysis focused on the pressure gradient as a function of the power set.

The results are presented in Figure 31, which shows the values obtained from the four experimental tests along with the corresponding regression curve.

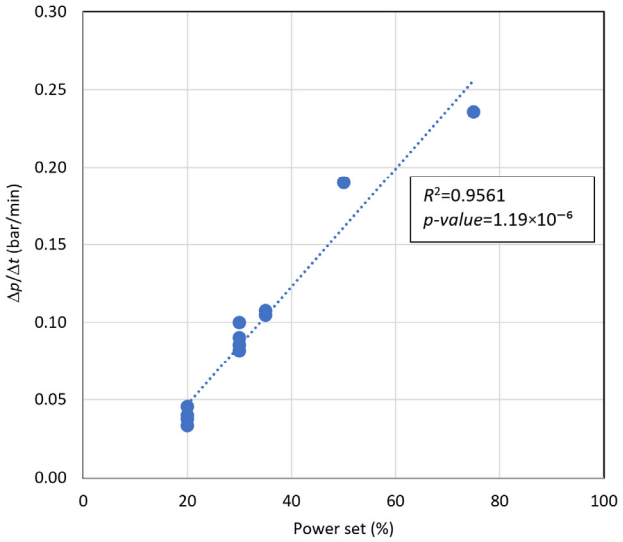

Figure 31. Pressure gradient—regression analysis.

The analysis of the figure reveals an approximately linear trend; the data were therefore interpreted using the following regression line:

$$\gamma = 0.0038\ PS - 0.0293 \quad (1)$$

where

- $\gamma = \Delta p/\Delta t$ (bar/min) is the pressure variation over time;
- PS (%) is the power set.

The correlation coefficient was found to be $R^2 = 0.9561$ and the p-value was calculated as 1.19×10^{-6}, indicating a result of high statistical significance.

This correlation is crucial for developing calibrated simulation models, which will be used to optimize and adapt the system to different contexts.

However, beyond the ascertained mathematical correlation, the observed behaviour also provides crucial insights into the system's operational performances, safety margins and process efficiency.

As a matter of fact, the pressure gradient ($\Delta p/\Delta t$) can be considered as an indicator of the hydrogen production rate. As expected, hydrogen generation increases with the power set, resulting in a faster pressure rise within the system. For instance, with a power set of 75%, the average pressure gradient reaches the value of 0.236 bar/min, which means that, under this condition, hydrogen is delivered to the tank for storage after about 75 min (after exceeding 17.5 bar). Considering that the process does not involve compression devices, this circumstance can be deemed as a satisfactory performance of the system.

In addition, the duration of this operation might be potentially reduced by lowering the pressure threshold which triggers the gas flow towards the tank.

However, such an adjustment would require a dynamic control strategy to ensure that the tank inlet pressure always exceeds the pressure of the stored hydrogen in order to

allow the gas flow toward the tank. This, in turn, implies the continuous monitoring of both storage pressure and hydrogen consumption. This aspect will be further investigated in the next phases of the research.

From a safety perspective, the pressurization phase is particularly critical. The threshold of 12 bar triggers the production phase, while the back-pressure valve opens at 17.5 bar, stabilizing the system pressure. The observed gradients, however, confirm a controlled and progressive increase within the system's design margins.

The rapid depressurization (up to 16.4 bar/min in Test 1) also highlights the system's ability to safely manage shutdowns and quickly return to ambient conditions. These findings suggest that, even under experimental conditions simulating a sudden production shutdown, the system maintains good operational stability and effectively executes emergency protocols.

Regarding efficiency, the pressure gradient can also be viewed as a qualitative measure of volumetric efficiency in the electrolysis process. Across tests, gradient variations are consistent with the supplied electrical power, suggesting that the input energy is effectively used for gas generation, with stable performance and no significant inefficiencies observed.

7. Conclusions

This study presented the design, operation, and experimental evaluation of a pilot-scale integrated system for green hydrogen production, purification, storage, and reconversion into electricity. The plant, powered primarily by a photovoltaic array, was tested under different operational configurations (on-grid and selective stand-alone) to evaluate its behaviour in real environmental conditions.

The experimental campaign provided a detailed insight into the system's dynamic performance across all process phases, from inerting to pressurization, production, and shutdown. The monitoring of key parameters, such as hydrogen pressure, oxygen concentration, electrolyser power input, and environmental variables, allowed the identification of critical performance trends and operational constraints.

A key outcome of the analysis is the identification of a strong linear correlation between the pressure gradient during the pressurization phase and the electrolyser power setpoint (R^2 = 0.9561). This relationship represents a valuable input for the calibration of simulation models, which will support predictive assessments and optimization strategies.

The collected data also pointed out some technical aspects, concerning the system's sensitivity to power fluctuations under selective stand-alone configuration and the challenges in maintaining stable operation at higher power levels when fully relying on renewable sources. Although further investigation is needed on this topic, and in this direction the development of the analysis has already been planned, these findings suggest the need for improved energy management and control strategies, especially when operating in stand-alone or selective stand-alone.

Overall, the experimental results demonstrate the feasibility of integrating renewable energy with hydrogen production systems at a small scale, while also revealing the key aspects that must be addressed to ensure stable, safe, and efficient operation. The insights gained from this work will inform future developments, including system scaling, energy optimization, and the implementation of advanced control algorithms.

In this context, a modular MATLAB-based simulation framework is already under development, built on the basis of the collected experimental data, to support predictive analysis and the design of improved operational strategies. MATLAB R2024a—version 24.1 (April 2024) is used. The model includes photovoltaic generation, battery dynamics, electrolyser operation, hydrogen storage, and fuel cell reconversion. It integrates the following:

- a phase-by-phase logic complying with the real system operation (e.g., purging, pressurization, depressurization);
- empirical correlations derived from experimental measurements;
- calibration and validation through dedicated test campaigns under different operational modes (on-grid and stand-alone).

This modelling approach will serve as the foundation for future work on control optimization and scenario simulation.

Author Contributions: Conceptualization, L.B., R.C., F.L.F., C.M., A.N., M.P., and M.V.; methodology, L.B., R.C., F.L.F., C.M., A.N., M.P., and M.V.; formal analysis, C.M. and A.N.; writing—original draft preparation, C.M. and A.N.; writing—review and editing, L.B., R.C., F.L.F., M.P., and M.V.; supervision, A.N. and M.P. All authors have read and agreed to the published version of the manuscript.

Funding: This research was funded by the European Union—Next Generation EU, Mission 4, Component 2, Investment 1.3—ASPIRE Project, Cascade Call of the PE NEST Program—Network 4 Energy Sustainable Transition (code PE00000021—CUP C39J24001350008).

Data Availability Statement: The raw data supporting the conclusions of this article will be made available by the authors on request.

Conflicts of Interest: The authors declare no conflicts of interest.

Abbreviations

The following abbreviations are used in this manuscript:

A-BSS	Auxiliary battery storage system
AWE	Alkaline water electrolyser
BSS	Battery storage system
DR	Drying unit
EM	Electrolyser
FC	Fuel cell
HB	Hydrogen storage tank
HC	Condenser
HD	Hydrogen buffer tank
HDO	Catalytic deoxidation reactor
HE	Hydrogen heat exchanger
HF	Separation filter
HI	Hybrid inverter
HO	Oxygen collection tank
HS	Hydrogen gas–liquid separator
HV	Hydrogen collection tank
HW	Hydrogen bubbler
MPPT	Maximum Power Point Tracker
OE	Oxygen heat exchanger
OS	Oxygen gas–liquid separator
OW	Oxygen bubbler
PEM	Polymer electrolyte membrane
PLC	Programmable logic controller
PV	Photovoltaic array
PV1; PV2	String 1 and 2 of the photovoltaic array
RES	Renewable energy sources
SOE	Solid oxide electrolyser
WT	Makeup water tank
WU	Demineralizer

References

1. Li, Y.; Liu, F.; Chen, K.; Liu, Y. Technical and Economic Analysis of a Hybrid PV/Wind Energy System for Hydrogen Refueling Stations. *Energy* **2024**, *303*, 131899. [CrossRef]
2. Marino, C.; Nucara, A.; Pietrafesa, M.; Pudano, A. An Energy Self-Sufficient Public Building Using Integrated Renewable Sources and Hydrogen Storage. *Energy* **2013**, *57*, 95–105. [CrossRef]
3. Maggio, G.; Nicita, A.; Squadrito, G. How the Hydrogen Production from RES Could Change Energy and Fuel Markets: A Review of Recent Literature. *Int. J. Hydrogen Energy* **2019**, *44*, 11371–11384. [CrossRef]
4. Europian Union Regulation (EU). 2021/1119 of the European Parliament and of the Council of 30 June 2021 Establishing the Framework for Achieving Climate Neutrality and Amending Regulations (EC) No 401/2009 and (EU) 2018/1999 ("European Climate Law"). *Off. J. Eur. Union L* **2021**, *243*, 1–17.
5. Guo, H.; Zhang, C.; Wang, J.; Wu, Z.; Wang, T.; Wang, P.; Qian, Y.; Zhang, G.; Yu, F. Design and Operation Schedule of RES Hydrogen Production System with Downstream Constraints. *Int. J. Hydrogen Energy* **2025**, *102*, 68–79. [CrossRef]
6. Arsad, A.Z.; Hannan, M.A.; Al-Shetwi, A.Q.; Begum, R.A.; Hossain, M.J.; Ker, P.J.; Mahlia, T.I. Hydrogen Electrolyser Technologies and Their Modelling for Sustainable Energy Production: A Comprehensive Review and Suggestions. *Int. J. Hydrogen Energy* **2023**, *48*, 27841–27871. [CrossRef]
7. Lazaroiu, G.; Gmal Osman, M.; Strejoiu, C.-V. Performance Evaluation of Renewable Energy Systems: Photovoltaic, Wind Turbine, Battery Bank, and Hydrogen Storage. *Batteries* **2023**, *9*, 468. [CrossRef]
8. Kang, Z.; Liu, S. Research on Capacity Optimization Configuration of Renewable Energy Off Grid Hydrogen Production System Considering Collaborative Electrolysis. *Energies* **2024**, *17*, 1962. [CrossRef]
9. Arunachalam, M.; Han, D.S. Efficient Solar-Powered PEM Electrolysis for Sustainable Hydrogen Production: An Integrated Approach. *Emergent Mater.* **2024**, *7*, 1401–1415. [CrossRef]
10. HassanzadehFard, H.; Tooryan, F.; Collins, E.R.; Jin, S.; Ramezani, B. Design and Optimum Energy Management of a Hybrid Renewable Energy System Based on Efficient Various Hydrogen Production. *Int. J. Hydrogen Energy* **2020**, *45*, 30113–30128. [CrossRef]
11. Bryan, J.; Meek, A.; Dana, S.; Islam Sakir, M.S.; Wang, H. Modeling and Design Optimization of Carbon-Free Hybrid Energy Systems with Thermal and Hydrogen Storage. *Int. J. Hydrogen Energy* **2023**, *48*, 39097–39111. [CrossRef]
12. Gökçek, M.; Paltrinieri, N.; Liu, Y.; Badia, E.; Dokuz, A.Ş.; Erdoğmuş, A.; Urhan, B.B.; Yoldaş, Ö. Optimum Sizing of Hybrid Renewable Power Systems for On-Site Hydrogen Refuelling Stations: Case Studies from Türkiye and Spain. *Int. J. Hydrogen Energy* **2024**, *59*, 715–729. [CrossRef]
13. Marino, C.; Nucara, A.; Panzera, M.F.; Pietrafesa, M.; Varano, V. Energetic and Economic Analysis of a Stand Alone Photovoltaic System with Hydrogen Storage. *Renew. Energy* **2019**, *142*, 316–329. [CrossRef]
14. Hou, J.; Yang, M. (Eds.) *Green Hydrogen Production by Water Electrolysis*; CRC Press: Boca Raton, FL, USA, 2024; ISBN 9781040047569.
15. da Rosa, A.V.; Ordóñez, J.C. (Eds.) Chapter 11—Hydrogen Storage. In *Fundamentals of Renewable Energy Processes*, 4th ed.; Academic Press: Oxford, UK, 2022; pp. 471–516, ISBN 978-0-12-816036-7.
16. Carmo, M.; Stolten, D. Chapter 4—Energy Storage Using Hydrogen Produced From Excess Renewable Electricity: Power to Hydrogen. In *Science and Engineering of Hydrogen-Based Energy Technologies*; de Miranda, P.E.V., Ed.; Academic Press: Cambridge, MA, USA, 2019; pp. 165–199, ISBN 978-0-12-814251-6.
17. Cirrincione, L.; Marino, C.; Nucara, A.; Panzera, M.F.; Pietrafesa, M.; Scaccianoce, G. Effect of the Accumulation Capacity on the Energy Performance of a Green Hydrogen Production Plant. In Proceedings of the 24th EEEIC International Conference on Environment and Electrical Engineering and 8th I and CPS Industrial and Commercial Power Systems Europe, EEEIC/I and CPS Europe 2024, Rome, Italy, 17–20 June 2024; pp. 1–6. [CrossRef]
18. Coralli, A.; Sarruf, B.J.M.; de Miranda, P.E.V.; Osmieri, L.; Specchia, S.; Minh, N.Q. Chapter 2—Fuel Cells. In *Science and Engineering of Hydrogen-Based Energy Technologies*; de Miranda, P.E.V., Ed.; Academic Press: Cambridge, MA, USA, 2019; pp. 39–122, ISBN 978-0-12-814251-6.
19. da Rosa, A.V.; Ordóñez, J.C. (Eds.) Chapter 9—Fuel Cells. In *Fundamentals of Renewable Energy Processes*, 4th ed.; Academic Press: Oxford, UK, 2022; pp. 317–417, ISBN 978-0-12-816036-7.
20. Ríos, C.; Molina, P.; Martínez de León, C.; Brey, J.J. Simulation of the Optimal Plant Size to Produce Renewable Hydrogen Based on the Available Electricity. *Int. J. Hydrogen Energy* **2024**, *52*, 1325–1337. [CrossRef]
21. Armijo, J.; Philibert, C. Flexible Production of Green Hydrogen and Ammonia from Variable Solar and Wind Energy: Case Study of Chile and Argentina. *Int. J. Hydrogen Energy* **2020**, *45*, 1541–1558. [CrossRef]
22. Hussam, W.K.; Barhoumi, E.M.; Abdul-Niby, M.; Sheard, G.J. Techno-Economic Analysis and Optimization of Hydrogen Production from Renewable Hybrid Energy Systems: Shagaya Renewable Power Plant-Kuwait. *Int. J. Hydrogen Energy* **2024**, *58*, 56–68. [CrossRef]

23. Dinh, V.N.; Leahy, P.; McKeogh, E.; Murphy, J.; Cummins, V. Development of a Viability Assessment Model for Hydrogen Production from Dedicated Offshore Wind Farms. *Int. J. Hydrogen Energy* **2021**, *46*, 24620–24631. [CrossRef]
24. Carbone, R.; Marino, C.; Nucara, A.; Panzera, M.F.; Pietrafesa, M. Electric Load Influence on Performances of a Composite Plant for Hydrogen Production from RES and Its Conversion in Electricity. *Sustainability* **2019**, *11*, 6362. [CrossRef]
25. Zou, P.; Lin, H.; Zhou, X.; Zou, Y.; Li, Y.; Yan, G.; Duan, X.; Cai, J. Control Strategies for Multi-Electrolyzer Alkaline Hydrogen Generation Systems Improving Renewable Energy Utilization and Electrolyzer Lifespan. *Renew. Energy* **2025**, *253*, 123628. [CrossRef]
26. Jinyong, X.; Yi, Z.; Mengru, X.; Minghui, Z. Optimal Configuration Method of Hydrogen Energy System for Coordinated Operation of Multi-Type Electrolyzers for New Energy Consumption. *Int. J. Hydrogen Energy* **2025**, *113*, 564–574. [CrossRef]
27. Bai, Z.; Hao, W.; Li, Q.; Yan, R.; Ding, B.; Shao, W.; Gao, L.; Jiang, T.; Wang, Y.; Wen, C. Enhancing Flexibility in Wind-Powered Hydrogen Production Systems through Coordinated Electrolyzer Operation. *Adv. Appl. Energy* 2025, *in press*. [CrossRef]
28. Raceanu, M.; Bizon, N.; Marinoiu, A.; Varlam, M. Design and Experimental Investigations of an Energy Storage System in Microgrids. In *Microgrid Architectures, Control and Protection Methods*; Tabatabaei, N.M., Kabalci, E., Bizon, N., Eds.; Springer International Publishing: Cham, Switzerland, 2020; pp. 207–232, ISBN 978-3-030-23723-3.
29. Wagner, E.; Delp, E.; Mishra, R. Energy Storage with Highly-Efficient Electrolysis and Fuel Cells: Experimental Evaluation of Bifunctional Catalyst Structures. *Top. Catal.* **2023**, *66*, 546–559. [CrossRef]
30. Patel, H.V.; Gorji, S.A.; Shahi, S.S.M.; Love, J.G. Implementation of a Lab-Scale Green Hydrogen Production System with Solar PV Emulator and Energy Storage System. In Proceedings of the 2021 11th International Conference on Power and Energy Systems, ICPES 2021, Shanghai, China, 18–20 December 2021; Institute of Electrical and Electronics Engineers Inc.: Piscataway, NJ, USA, 2021; pp. 201–208.
31. Folgado, F.J.; Orellana, D.; González, I.; Calderón, A.J. Processes Supervision System for Green Hydrogen Production: Experimental Characterization and Data Acquisition of PEM Electrolyzer. *Eng. Proc.* **2022**, *19*, 36. [CrossRef]
32. Raimondi, G.; Spazzafumo, G. Integrating Renewable Energy Communities and Italian UVAM Project through Renewable Hydrogen Chain. *e-Prime-Adv. Electr. Eng. Electron. Energy* **2024**, *10*, 100819. [CrossRef]
33. Bagheri, B.; Kumagai, H.; Hashimoto, M.; Sugiyama, M. Techno-Economic Assessment of Green Hydrogen Production in Australia Using Off-Grid Hybrid Resources of Solar and Wind. *Energies* **2025**, *18*, 3285. [CrossRef]
34. Westman, J.; Hadidi, R. Overload Mitigation for Grid-Forming Inverters in Islanded Microgrids with Synchronous Generators. *Electr. Power Syst. Res.* **2025**, *239*, 111231. [CrossRef]
35. Serban, I. A Control Strategy for Microgrids: Seamless Transfer Based on a Leading Inverter with Supercapacitor Energy Storage System. *Appl. Energy* **2018**, *221*, 490–507. [CrossRef]
36. AbdelAty, A.M.; Al-Durra, A.; Zeineldin, H.; El-Saadany, E.F. Improving Small-Signal Stability of Inverter-Based Microgrids Using Fractional-Order Control. *Int. J. Electr. Power Energy Syst.* **2024**, *156*, 109746. [CrossRef]
37. Yorino, N.; Sekizaki, S.; Adachi, K.; Sasaki, Y.; Zoka, Y.; Bedawy, A.; Shimizu, T.; Amimoto, K. A Novel Design of Single-Phase Microgrid Based on Non-Interference Core Synchronous Inverters for Power System Stabilization. *IET Gener. Transm. Distrib.* **2023**, *17*, 2861–2875. [CrossRef]